

Optimally estimating Granger causality

Qiang Luo^{1,†}, Wenlian Lu^{2,3†}, Wei Cheng^{2,4,†}, Pedro A. Valdes-Sosa⁵, Xiaotong Wen⁶,
Mingzhou Ding⁶ and Jianfeng Feng^{2,3,*}

¹Department of Management, School of Information Systems and Management, National University of
Defense Technology, Hunan 410073, P.R. China

²Centre for Computational Systems Biology, School of Mathematical Sciences, Fudan University,
Shanghai 200433, P.R. China

³Centre for Scientific Computing, University of Warwick, Coventry CV4 7AL, United Kingdom

⁴Mathematical Department, Zhejiang Normal University, Jinhua, 321004, Zhejiang Province, PR
China

⁵Cuban Neuroscience Center, Ave 25 #15202 esquina 158, Cubanacan, Playa, Cuba

⁶J. Crayton Pruitt Family Department of Biomedical Engineering, University of Florida, Gainesville,
Florida, US

[†] These authors contributed to this work equally.

^{*} Correspondence should be addressed to Jianfeng Feng, Fudan University, Shanghai 200433, P.R. China. E-mail:
jianfeng64@gmail.com.

Abstract

It is a rule, rather than an exception, that physiological oscillations of various frequencies are present in fMRI signals. Here we presented a theoretical framework to show how to more reliably and precisely estimate Granger causality from experimental datasets with time-varying properties caused by the physiological oscillations. Within this framework, the Granger causality was redefined as a global index measuring directed information flow between time series with the time-varying properties. Both theoretical analyses and numerical examples demonstrated that the Granger causality is an increase function of the temporal resolution used in estimation, reflecting the general physics principle of coarse graining, which causes information loss by smoothing out very fine-scale details both in time and space. This was also confirmed by results that the Granger causality on the finer spatial-temporal scales considerably outperforms the traditional approach in terms of the improved consistency between two resting-state scans for the same subject. For practice, the proposed theoretical framework was implemented by combining together several modules, including the optimal time window dividing, parameter estimation in the fine temporal and spatial scales to optimally estimate the Granger causality. Taking together, our approach provided a novel and robust framework to estimate the Granger causality from the fMRI, EEG and related data.

Introduction

Granger causality, a standard statistical tool for detecting directional influence between system components, plays a key role in understanding system behaviours in many different areas, including finance (Chen et al., 2011), climate (Evan et al., 2011), genetics (Zhu et al., 2010) and neuroscience (Ge et al., 2012; Ge et al., 2009; Guo et al., 2008; Luo et al., 2011). The basic idea of Granger causality was originally proposed by Wiener in 1956 (Wiener, 1956), and introduced into data analysis in by Granger in 1969 (Granger, 1969). This idea can be briefly described as follows: If the historical information of time series A significantly improves the prediction accuracy of the future of time series B in a multivariate auto-regression (MVAR) model, then the Granger causality from time series A to B is identified. In the classic Granger causality, time-invariant MVAR models are used to fit the observed time series experimental data.

However, a time-varying property is a common phenomenon in various systems. For example, the gene regulatory network in *Saccharomyces cerevisiae* was reported by Luscombe et al. (Luscombe et al., 2004) to evolve the topologies, with respect to different stimuli, or different life processes. A time-varying protein-protein interaction network for p53 was found by Tuncbag et al. (Tuncbag et al., 2009), who hence suggested the 4D view of the protein-protein interaction network with time as the 4th dimension. In the primary visual cortex of anaesthetized Macaque monkeys, ensembles of neurons have dynamically reorganized moment-to-moment effective connectivity (Ohiorhenuan et al., 2010). The importance of a slow oscillation such as the theta rhythm in a neuronal system is analysed in (Smerieri et al., 2010). It should be pointed out that even if the time series of data were observed to be weakly stationary (i.e., stationary in the second moment), the configuration of the system could be time-varying. A typical example is $X_t = a \cos(\omega t + U_t) + \xi_t$, where t is time, a and ω are constants, $U_t \sim U[-\pi, \pi]$ is a uniform distribution, and ξ_t is noise. It is thus natural to consider time-varying systems and understand their impacts on the

estimation of the Granger causality.

Recently, analysing systems with time-varying structures has attracted increasing interest and many statistical methods have been proposed. Let us mention a few of these. An adaptive multivariate autoregressive model via sliding short time windows was proposed by (Ding et al., 2000) to deal with a non-stationary, event-related potential (ERP) time series. A short time window approach was used by (Hesse et al., 2003) to define time-dependent Granger causalities for inspecting directed interdependencies of Electroencephalography (EEG) data. The time-varying Granger causality has also been modelled by Markov-Switching models in (Psaradakis et al., 2005; Warne, 2000). In these models, the time-varying Granger causality was modelled by a hidden discrete Markov process with finite state space. A wavelet-based time-varying Granger causality was suggested in (Sato et al., 2006) to establish the functional connectivity maps from fMRI data. A time-varying model based on the Ising model was applied to both biological and social networks in (Ahmed and Xing, 2009), but this model does not provide the directional information of the time-varying relationship between variables. The dual Kalman filter was used in (Havlicek et al., 2010; Sommerlade et al., 2012) to estimate the time-dependent coefficients in the MVAR model for inferring the time-variant Granger causality between non-stationary time series. These approaches extended the classic Granger causality inference to the non-stationary case via adaptive multivariate autoregressive modelling. However, the more sophisticated the model is, the more preconditions may be required for the data. For example, the independent and identical distributed condition for the observed data by the Bayesian network, the effective connectivity can be modelled by random walk in time-variant Granger causality, the first and second order smoothness of the underlying time-varying properties, etc. Different from the literature that dealt with the time-varying properties in MVAR model and defined Granger causality as a function with respect to time, we are to propose a robust *global* index measuring the directed information flow between time series, despite of the time-varying properties. Granger causality is now a popular model for

this purpose, but the classic Granger causality does not consider the time-varying properties in data. Moreover, the idea that the longer the time series we have, the more reliable the result we are able to obtain for Granger causality is pervasive in practice.

When studying Granger causality in resting-state fMRI, its reliability has engendered a number of disputes recently. In the literature, it has always happened that some directional information transferring, that was inferred by one paper, based on a set of data, cannot be repeated in another paper, based on another or even the same set of data. This casts doubts on the efficiency and validity of the Granger causality. The possible reasons have been widely investigated by many authors. In (Friston et al., 1995), the authors used hemodynamics to model the underlying neural activities, so the Granger causality should be analysed at the neural activity level. Additional, more detailed discussions were presented in (Smith et al., 2012). Actually, there are also many researches manifested the validity of Granger causality against the confounding factor of hemodynamic function (HRF). In (Deshpande et al., 2010), the authors convolved the HRF with the local field potentials (LFP) recorded from the macaque, and found that even if the HRF delays opposed neuronal delays the minimum detectable neuronal delay was still as short as hundreds of milliseconds. Most recently, Schippers et al. (2011) had done another simulation based investigation on the same issue, and found that Granger causality can successfully detect over 80% of the cases when the influences flowing to a region with a faster hemodynamic delay if the neuronal delays were above 1s. As concluded by the authors in (Schippers et al., 2011), if a significant Granger causality is detected, ‘this finding is unlikely to have arisen without a true underlying information flow between these regions. Given the complex nature of the brain system, the more we understand the system the more we need to improve our modeling methods, particularly the Granger causality analysis.

The aims of this paper were the following twofold.

(1) We aimed to answer the question, what is the impact of the temporal scale in the

MVAR models on the resulting directional influence of Granger causality? For Gaussian variables, the Granger causality is equivalent to the directed information transfer between variables. Hence the question is how the temporal scale in the MVAR model influences the estimation of the information flows between each variable within a system. In (Smith et al., 2011), the authors compared the performances of Granger causality analysis on simulations with different time lengths, and found that the longer the time series was the better the performance could be. However, in their simulations the underlying circuit stayed the same during the simulation. In this paper, we are going to investigate the effects of the time-varying underlying circuits on the Granger causality analysis both mathematically and empirically. Mathematically, consider two time series x and y over a time window $[0, T]$. A *change-point set* $S_1 = \{0 = t_0 < t_1 < \dots < t_m = T\}$ defines the time-varying property of the MVAR model as follows: at each time window $[t_{k-1}, t_k)$, the MVAR model is static, i.e., the coefficients of the directional influence between variables are constant, but different time windows may have different MVAR models. Thus, it becomes a time-varying MVAR (TV-MVAR). There are two alternative ways to estimate the Granger causality from y to x in the TV-MVAR model with respect to the change-point set S_1 . One is to estimate the local Granger causality at each time window $[t_{k-1}, t_k)$ and then average them, termed *average Granger causality*, $F_{y \rightarrow x}^{(a, S_1)}$. The other is to average the variances of the residual errors locally at each small time window, and then, the *cumulative Granger causality*, $F_{y \rightarrow x}^{(c, S_1)}$, can be established by comparing the estimated variances of residual errors of x by considering y or not to predict the future of x . The TV-MVAR model depends on the change-point set that can be divided into finer time windows, as shown in Figure 1. Hence, we needed to address what the relationships are of these various definitions of causality with respect to the fineness of the change-point set in the TV-MVAR model.

We proved that both the cumulative Granger causality and the average Granger causality are in general monotonically increasing functions with respect to the change-point set (see Figure 1 for a summary). That is, the finer the TV-MVAR model is, namely, the larger the change-point set is, the larger (average and cumulative) Granger causalities are estimated. In particular, as shown in Theorems B1 and B4, under our assumption, in the coarser MVAR model, the estimation of the coefficients is the (weighted) average of those of the finer model. So, if the “true” time-varying coefficients are nonzero but have their signs fluctuating, then the “averaging” estimation may reduce their absolute values due to the neutralisation. This may increase the probability of incorrect inference of Granger causality.

(2) The second aim of this paper is to provide an efficient algorithm to estimate the global Granger causality index for an arbitrary pair of given time series without any prior knowledge of the MVAR model involved. It should be emphasised that there is a trade-off for the window length of the change points in the TV-MVAR model. It cannot be too small to give a reliable estimation of the parameters; on the other hand, too large time windows might increase the probability to give an incorrect inference of the Granger causality. Based on Bayesian information criterion (BIC) and a change-point searching algorithm, we proposed an algorithm to search for optimal change-point in order to achieve the optimisation and trade-off between the details of the Granger causality and the accuracy of the model estimation. The theoretical results and the proposed algorithm were verified by estimating the average and cumulative Granger causalities on both simulated and experimental data. Both results reinforced the theoretical conclusion that the finer change-point set gives the larger overall causality measurement.

To investigate the test/retest reliability of Granger causality established by our model, we computed Pearson’s correlation coefficients for the Granger causality patterns across two scanning series on the same subject from the enhanced Nathan Kline Institute-Rockland Sample (see Materials and Methods). By taking finer details in the

TV-MVAR model both temporally and spatially in the fMRI data, the Granger causality had much better consistency results across two scan sessions for the same subject. In particular, the correlation coefficient increased from 0.3588 by the classic Granger causality with static MVAR model and region-wise estimation, considerably to 0.6059 by our approach, including optimal TV-MVAR model and voxel-wise estimation.

Furthermore, on a data set of resting-state fMRI time series, a Granger causality estimate, based on the static MVAR model for the whole time interval, failed to identify any significant causal connectivity for the precuneus. In comparison, within a finer-scale for the TV-MVAR model, Granger causality told us that the precuneus is served as a hub. Information flows between the precuneus and the visual regions were also revealed which was inconsistent with the experimental setting that the data were collected with subjects' eyes open. On a data set of task-associated fMRI time series, the average Granger causality estimated for the attention blocks were found significantly larger than those estimated by the classic Granger causality based on static MVAR model for the whole time series for all 12 subjects in the experiment.

The estimation of Granger causality is heavily influenced by the model. Our results showed that a coarse-grained approach/model may average out the meaningful information, as echoed in the idiom 'the devil is in the details'. The general belief that the longer the data set is recorded, the better we can estimate the statistics (here it is Granger causality), is not true if the whole long-term time series are all taken into the coarse-grained MVAR model, for example, a static MVAR model. Instead, we suggest, in this paper, that the optimal strategy is to divide the long-term recording into a number of time windows either by comparing the BIC's among models with different time window lengths or an optimal BIC-based algorithm. Reliable estimation of the Granger causality by a finer-scale MVAR model both in time and space can be achieved.

Materials and Methods

Simulation Dataset for monotonicity of Granger causality

Consider two time series and the effective interdependencies between them were described by the TV-MVAR model with constant noise level. In reality, the data of time-series were generated by the following toy model

$$\begin{pmatrix} x^{t+1} \\ y^{t+1} \end{pmatrix} = \begin{pmatrix} A_{11}(t) & A_{12}(t) \\ A_{21}(t) & A_{22}(t) \end{pmatrix} \begin{pmatrix} x^t \\ y^t \end{pmatrix} + \begin{pmatrix} n_{xy}^t \\ n_{yx}^t \end{pmatrix}, \quad (1)$$

where

$$A_{11}(t) = 0.1, A_{12}(t) = 0.5 \left(\frac{t}{600} - 1 \right) \cdot u_1$$
$$A_{21}(t) = 0.5 \left(1 - \frac{t}{400} \right) \cdot u_2, A_{22}(t) = 0.1\sqrt{2}$$

We generated 100 toy models by randomly setting the parameters u_1 and u_2 according to the uniform distribution on the interval of $[0,1]$. For each model, the time series observations were generated for 1200 time steps. The parameters A_{12} and A_{21} are the corresponding causal coefficients for the causal influences at the directions $Y \rightarrow X$ and $X \rightarrow Y$, respectively. Nonzero causal coefficient means the causal influence at the corresponding direction. In this simulation, the causal coefficient changed from positive to negative.

Simulation Dataset for significance of Granger causality

Consider a TV-MVAR model of two components with only one directional causal influence, $X \rightarrow Y$, by setting the corresponding coefficient A_{21} to have non zero values during the time course. The model came from Equation (1) with the step-wise coefficients as follows

$$A_{11}(t) = 0.1, A_{22}(t) = 0.1\sqrt{2},$$

$$A_{12}(t) = 0, A_{21}(t) = \begin{cases} 0.5u_1, & 0 < t \leq t_1 \\ 0, & t_1 < t \leq t_2 \\ -0.5u_1, & t_2 < t \leq t_3 \\ 0, & t_3 < t \leq T \end{cases} \quad (2)$$

where $t_1 = 215$, $t_2 = 415$ and $t_3 = 715$. We generated two time series with 1200 time points and repeated this generation 100 times by randomly setting the parameter u_1 from a uniform distribution on the interval of $[0.5, 1.5]$. In this simulation, the causal coefficient A_{12} for the direction $Y \rightarrow X$ is set to be zero, so no causal influence from Y to X ; the causal coefficient A_{21} changed across different time windows.

Multiband Imaging Test-Retest Pilot Dataset

This set of fMRI data was from the enhanced Nathan Kline Institute-Rockland Sample. The whole dataset consisted of resting-state fMRI recordings in two sessions for 17 subjects (healthy, ages 19-57, and 4 females).

The fMRI data were collected using 3 Tesla and 40 slices were acquired for 900 volumes. Multiband echo planar Imaging approaches enable the acquisition of fMRI data with unprecedented sampling rates ($TR=0.645s$) for full-brain coverage through the acquisition of multiple slices simultaneously in the same time. For more detailed information about this data set, please see the website http://fcon_1000.projects.nitrc.org/indi/pro/eNKI_RS_TRT/FrontPage.html.

Data pre-processing was performed by the DPARSF software (Yan and Zang, 2010). The first 50 volumes were discarded to allow for scanner stabilisation. Since multiple slices were excited simultaneously, simple slice time correction might not work well. Given the short effective TR it is probably less important, so it is omitted in our data pre-processing. After the realignment for head-motion correction, the standard Montreal Neurological Institute (MNI) template provided by SPM2 was used for spatial normalization with a re-sampling voxel size of $3 \times 3 \times 3 \text{ mm}^3$. After smoothing

(FWHM=8mm), the imaging data were temporally filtered (band pass, 0.01~0.08Hz) to remove the effects of very low-frequency drift and high-frequency noises (e.g., respiratory and cardiac rhythms). An automated anatomical labelling (AAL) atlas (Tzourio-Mazoyer et al., 2002) was used to parcellate the brain into 90 regions of interest (ROIs). To verify the principle of voxel-level Granger causality, the brain were also divided into 1024 ROIs with around 45 voxels each according to a high-resolution brain atlas provided by (Zalesky et al., 2010).

Resting-State fMRI Dataset

The resting-state fMRI data set was a subset of a large database, called “1000 Functional Connectomes Project” (Biswal et al., 2010), which was freely accessible at the website: www.nitrc.org/projects/fcon_1000/. Here, the dataset provided by Buckner’s group at Cambridge, USA, was used for the present study. This data set consists of 198 healthy subjects (75 males, 123 females and ages 18-30). The fMRI data (TR = 3s) were collected using 3 Tesla and 47 slices were acquired for 119 volumes. More detailed information about this data set can be found on the website mentioned above.

The first 5 volumes were discarded to allow for scanner stabilization. The DPARSF(Yan and Zang, 2010) based on SPM8 was used for pre-processing the fMRI data, including slice-timing correction, motion correction, co-registration, grey/white matter segmentation, and spatially normalization to Montreal Neurological Institute (MNI) space and resampled to $3 \times 3 \times 3 \text{ mm}^3$. The waveform of each voxel was detrended and passed through a band-pass filter from 0.01 Hz to 0.08 Hz. The data were smoothed spatially (FWHM=8 mm). In results, the time series data with 114 time points of 90 brain regions (AAL-atlas) for 198 subjects were achieved.

fMRI Dataset for Attention-Task

The dataset of fMRI time series for an attention-task experiment was provided by Ding Group at the University of Florida, USA (Wen et al., 2012), which consisted of

12 subjects who successfully completed the task (8 females, 4 males, ages 20-28). This experiment adopted a mixed blocked/event-related design. There were 12 attention blocks and 12 passive-view blocks, together with some fixation intervals. In each attention block, the subject performed a trial-by-trial cued visual spatial attention task. The fMRI data were collected using 3 Tesla and 33 slices were acquired for 180 volumes for each of the six runs with TR 2s. The data set was pre-processed by slice timing, motion correction, co-registration to individual anatomical image, normalization to the Montreal Neurological Institute (MNI) template, and resampled to $3 \times 3 \times 3 \text{ mm}^3$, using DPARSF. The hemodynamic response function (HRF) was convolved by the blocked rectangular function corresponding to a given experimental condition during the GLM analysis. For more detailed information about this dataset, please see(Wen et al., 2012).

For each attention block, there were 30 data points, lasting for 60 seconds. The task average response was removed from each attention block by subtracting the mean of the time series data across 12 attention blocks. The first 5 data points (10 seconds) were discarded to eliminate transient effects. The temporal mean was removed for each attention block to meet the zero mean requirement of the Granger causality analysis. Therefore, we had 300 data points for the 12 attention blocks. Here, the causality between the right intra-parietal sulcus (rIPS) and the right temporal-parietal junction (rTPJ) was studied. There were time series for 19 voxels and 17 voxels for the rIPS and rTPJ respectively (Wen et al., 2012).

Granger causality in TV-MVAR

For two time series x^t and y^t with $t = 1, 2, \dots, T$. Define a change-point set as an increasing integer series: $1 = t_0 < t_1 < \dots < t_{m-1} < t_m = T + 1$, denoted by S_1 . Consider the following piece-wise constant linear system to describe the directional influence from y^t to x^t as follows:

$$x^{t+1} = \bar{a}_1^{S_1}(k)x^t + \bar{b}_1^{S_1}(k)y^t + n(t), t_{k-1} \leq t < t_k, k = 1, \dots, m \quad (3)$$

where $\bar{a}_1^{S_1}(k)$ and $\bar{b}_1^{S_1}(k)$ are estimated time-varying coefficients, due to S_1 . Also,

if ignoring the directed causality from y^t to x^t , then the system (3) becomes

$$x^{t+1} = \tilde{a}_1^{S_1}(k)x^t + \tilde{n}(t), t_{k-1} \leq t < t_k, k = 1, \dots, m \quad (4)$$

where $\tilde{a}_1^{S_1}(k)$ is the estimated time-varying coefficient in this model. At the k^{th} time

window, the Granger causality can be defined locally as

$$F_{y \rightarrow x}^{(k, S_1)} = \log \left[\frac{\sum_{t=t_{k-1}}^{t_k-1} \text{var}(\tilde{n}(t))}{\sum_{t=t_{k-1}}^{t_k-1} \text{var}(n(t))} \right].$$

The average Granger causality with respect to S_1 can be estimated by the average of Granger causalities at the time windows and weighted by the corresponding window lengths:

$$F_{y \rightarrow x}^{(a, S_1)} = \frac{1}{T} \sum_{k=1}^m F_{y \rightarrow x}^{(k, S_1)} (t_k - t_{k-1}) \quad (5)$$

If the length of each time window is uniform, it becomes

$$F_{y \rightarrow x}^{(a, S_1)} = \frac{1}{m} \sum_{k=1}^m F_{y \rightarrow x}^{(k, S_1)}.$$

The other way to compute the Granger causality is cumulating the residual square errors across all time windows. This is called the cumulative Granger causality with respect to S_1 and can be estimated as:

$$F_{Y \rightarrow X}^{(c, S_1)} = \log \left[\frac{\sum_{t=1}^T \text{var}(\tilde{n}(t))}{\sum_{t=1}^T \text{var}(n(t))} \right] = \log \left[\frac{\sum_{k=1}^m \sum_{t=t_{k-1}}^{t_k-1} \text{var}(\tilde{n}(t))}{\sum_{k=1}^m \sum_{t=t_{k-1}}^{t_k-1} \text{var}(n(t))} \right]. \quad (6)$$

In particular, if the random variable y^t is stochastically orthogonal to x^t at each time,

i.e., $E \left[(x^t - Ex^t)(y^t - Ey^t) \right] = 0$ for all t , then the cumulative Granger causality can be

estimated as:

$$F_{Y \rightarrow X}^{(c, S_1)} = \log \left[\frac{\sum_{k=1}^m \sum_{t=t_{k-1}}^{t_k-1} [a_1(t) - \tilde{a}_1^{S_1}(k)]^2 \text{var}(x^t) + \sum_{k=1}^m \sum_{t=t_{k-1}}^{t_k-1} [b_1(t)]^2 \text{var}(y^t) + \sum_{k=1}^m \sum_{t=t_{k-1}}^{t_k-1} \text{var}(n(t))}{\sum_{k=1}^m \sum_{t=t_{k-1}}^{t_k-1} [a_1(t) - \bar{a}_1^{S_1}(k)]^2 \text{var}(x^t) + \sum_{k=1}^m \sum_{t=t_{k-1}}^{t_k-1} [b_1(t) - \bar{b}_1^{S_1}(k)]^2 \text{var}(y^t) + \sum_{k=1}^m \sum_{t=t_{k-1}}^{t_k-1} \text{var}(n(t))} \right].$$

For the details of the derivative of the expressions for the Granger causalities, please see Appendix A. Here, only the first-order regression model with one-dimensional variables is considered, but the approach and results work for general high-order and high dimensional TV-MVAR model that will appear in our near future paper.

Since in each time window $F_{y \rightarrow x}^{(k, S_1)}$ obeys F -distribution after proper scaling, the average Granger causality defined above can be considered in the null hypothesis as the summation of m independent F -distributed random variables whose degree-of-freedoms can be given according to the number of free parameters and the length of each time window, particularly, 1 and $t_k - t_{k-1} - 3$. Therefore, the p -value for the significance of the average Granger causality can be calculated. Similarly, the cumulative Granger causality defined above also obeys the F -distribution with the degree-of-freedom, m and $T-2m-1$.

Optimal time window dividing

In practice, the true time-varying structure of the data is generally unknown, i.e. we do not know the how many change-points and how long of each time window are necessary to describe the data. Therefore, an algorithm for dividing the time series into many time windows with variable lengths to better describe the data is required. Equivalently, we want to search for the optimal change-point set. The optimal time-window dividing means a trade-off between the satisfactory accuracy of the model parameter estimation and the lossless causal information established by the model. Mathematically, considering the following step-wise TV-MVAR model

$$X(t+1) = \sum_{k=1}^m a_1^k X(t) I_{[t_{k-1}, t_k]} + n(t), \quad (7)$$

where $I_{[t_{k-1}, t_k]}$ is the characteristic function of the time window $[t_{k-1}, t_k]$, $n(t)$ is the

Gaussian white noise term, a_1^k represents the (constant) coefficient in the k^{th} interval, and

$$S(m) = \{t_1, \dots, t_{m-1} \mid 1 = t_0 < t_1 < \dots < t_{m-1} < t_m = T + 1\}$$

is the change-point set. Given the change-points, the model can be fitted in each time window as \hat{a}_1^k , and the variance of the residual errors can also be estimated for each time window, denoted by $\hat{\Sigma}_k$. Therefore, the accuracy of the model can be defined by the weighted average of the variances of the residuals in each time window as follows:

$$err(S(m)) = \frac{1}{m} \sum_{k=1}^m (t_k - t_{k-1}) \det(\hat{\Sigma}_k). \quad (8)$$

On the other hand, the information captured by this model can be measured by the average Granger causality in all directions defined in the previous section, noted by

$$agc(S(m)) = \frac{1}{2m} \sum_{k=1}^m (F_{y \rightarrow x}^{(k, S(m))} + F_{x \rightarrow y}^{(k, S(m))}). \quad (9)$$

To minimize the prediction error and maximize the detected causality information, the optimal window dividing can be derived by optimising the following cost function with a trade-off parameter λ

$$S_{opt}(m, \lambda) = \arg \min_{S(m)} err(S(m)) + \lambda / agc(S(m)). \quad (10)$$

To determine the trade-off parameter, we can find the optimal change-point set $S_{opt}(m, \lambda)$ for different $\lambda \in [\lambda_1, \lambda_2]$ and calculate the Bayesian information criterion (BIC) for this change-point set as follows:

$$BIC(m, \lambda) = -2 \sum_{k=1}^m LLF_k + 2^2 m \log(T + 1) \quad (11)$$

where LLF_k stands for the log likelihood function established for the k^{th} window. Searching for the optimal change-point set with a series of given the number of time windows, $m \in [0, 1, 2, \dots, m_0]$, and trade-off parameter, $\lambda \in [\lambda_1, \lambda_2]$, is the first step; the second step is to compare the BIC values established by different change-point

sets generated from the first step, and then the one with the smallest BIC is selected to define the optimal time window. Therefore, with fixed upper bound of the number of time windows, m_0 , the algorithm for optimal time window dividing is described as follows:

Algorithm for optimal time window dividing

For $\lambda =$ from λ_1 to λ_2

For $m =$ from 1 to m_0

Establish $S_{opt}(m, \lambda)$ by optimizing Eq. (10)

End

Calculate BIC for each $S_{opt}(m, \lambda)$ by Eq. (11)

End

Find the optimal $S_{opt}(m_{opt}, \lambda_{opt})$ with the smallest BIC

Temporal-spatial Granger causality

Furthermore, both spatial and temporal fineness were taken into the MVAR model. The idea of spatial finer-scale for Granger causality estimation was similar to the time-varying Granger causality we mentioned above. Consider a dataset of fMRI BOLD signals from m voxels in ROI A and n voxels in ROI B. For each pair of voxels in these two ROIs respectively, the Granger causality between the voxel pair was calculated for each subject, denoted by F_{ij} from the i th voxel in ROI A to the j th voxel in ROI B; and then the *global* Granger causality from region A to B, namely *voxel-level Granger causality*, is defined as:

$$F_{A \rightarrow B} = \frac{1}{mn} \sum_{i \in ROI_A} \sum_{j \in ROI_B} F_{ij}.$$

Furthermore, the temporal and the spatial fine-scale were combined together to give

optimal estimation of Granger causality by looking into the temporal details for each pair of voxels, called the *spatial-temporal Granger causality*:

$$F_{A \rightarrow B}^{(e,S)} = \frac{1}{mn} \sum_{i \in ROI_A} \sum_{j \in ROI_B} F_{ij}^{(e,S)},$$

with $e = a$ or c for average and cumulative (time-varying) Granger causality respectively. In comparison, the classic Granger causality usually estimates the causality between two ROIs by averaging the time series data among all voxels for each ROI with a static MVAR model.

Results

Monotonicity of Granger causality with respect to change-point set

Used the simulation dataset for the monotonicity test of Granger causality and each time series had a length of 1200 time steps. Three different time window lengths, 50, 200, and 400, were used, of which the corresponding change-point sets were denoted as $S_i, i = 1, 2, 3$, respectively. Theorems B1 and B4 in Appendix B show that

$$F_{Y \rightarrow X}^{a,S_1} \geq F_{Y \rightarrow X}^{a,S_2} \geq F_{Y \rightarrow X}^{a,S_3} \text{ and } F_{Y \rightarrow X}^{c,S_1} \geq F_{Y \rightarrow X}^{c,S_2} \geq F_{Y \rightarrow X}^{c,S_3} \text{ hold if the parameters are precisely}$$

estimated since $S_1 \supset S_2 \supset S_3$. To demonstrate that, the 95% confidence intervals of

$$D_1^a = F_{Y \rightarrow X}^{a,S_1} - F_{Y \rightarrow X}^{a,S_2}, D_2^a = F_{Y \rightarrow X}^{a,S_2} - F_{Y \rightarrow X}^{a,S_3} \text{ and } D_3^a = F_{Y \rightarrow X}^{a,S_1} - F_{Y \rightarrow X}^{a,S_3} \text{ were established for}$$

the causality results in 100 runs of the simulation toy model. Similarly, $D_i^c, i = 1, 2, 3$ were defined and their confidence intervals were established, too. From Table 1, we can see that the estimated Granger causality for the same pair of time series decreases as the length of the time window becomes longer. That is, the more change-points are used in the TV-MVAR model, i.e., the finer the model is, the larger the Granger causality can be estimated for the same time series.

In particular, as shown in Theorems B1 and B4, under our assumption, in the coarser MVAR model, the estimation of the coefficients is the (weighted) average of those of the finer model. By algebraic inequalities, the monotonicity can be proved. As an

intuitive interpretation, if the “true” time-varying coefficients are nonzero but have their signs fluctuating, for example, it equals to 1 at the first time interval and -1 at the last time interval with equal length, and then the “averaging” estimation becomes zero, in the case that the coefficient parameters are precisely estimated, due to the neutralisation. Thus, in the static MVAR model, ideally, we will infer that there is no Granger causality despite that it does have. The similar argument can work for the comparison of finer and coarser MVAR models. Therefore, the coarser MVAR model might increase the probability of incorrect inference of the information transfer between time series.

To show the accuracies of the model estimation, we compared the differences between the variances of the model residual errors estimated for the static MVAR model by the whole time series, denoted by $Err_{[1,1200]}$, and the average variances of the model residual errors for the TV-MVAR model over time windows, $\overline{Err_{S_i}}$, as $D_i = Err_{[1,1200]} - \overline{Err_{S_i}}$ for $i=1,2,3$. As shown in Figure 2A, the TV-MVAR models with different time-window lengths all have smaller variances than the static MVAR model fitted on the whole time series for all 100 toy models, i.e., the $D_i > 0$ holds for 100 runs of the toy model. Among the models with different time window sets, the one with the smallest length of the time window, i.e., which had S_1 as the change-point set, gave the most accuracy estimation of the simulated time series.

Significance of Granger causality

We compared the significance of the results detected by our time-varying Granger causality approach with those by the classic Granger causality. If the p -value was lower than a threshold, a significant directional influence was detected. In this simulation setup, the causal influence did exist from X to Y , but did not from Y to X . Used the usual definitions of the truth positive (TP), false positive (FP), truth negative (TN) and false negative (FN), and set the maximum number of the time windows

$m_0 = 5$ and the trade-off parameter ranging from $\lambda_1 = 0.02$ to $\lambda_2 = 1$ with the step size 0.02. Five types of Granger causalities, including the classic Granger causality (classic GC), the average Granger causality (average GC), the cumulative Granger causality (cumulative GC), the average Granger causality with optimally divided time windows (Opt average GC), the cumulative Granger causality with optimally divided time windows (Opt cumulative GC) were calculated on the simulation data for significance test and the results are listed in Table 2.

The classic GC without considering the time-varying property of the underlying structure of the data failed to identify any causal influence between these two time series. The introduced cumulative GC and average GC gave better results in terms of higher TP rate and TN rate than the classic GC did. Compared to the other algorithms, the average GC and the cumulative GC with optimally divided time windows gave the best performance in terms of the TP rate and the TN rate.

The cumulative GC and the average GC used the time windows with equal lengths, and the better performances achieved by these two algorithms when their time window lengths were similar to the real structure of the simulated data. Since the real change-points of this simulation were 215, 415 and 715, both the algorithms gave better results when the lengths of time windows were 100 or 300, and the performances became worse when the time windows had longer or shorter lengths.

The false positive rates were zero for both the cumulative GC and the average GC with different window lengths when we used the threshold of significance as $1e-11$ for the F statistics. Therefore, the FP rates of these two algorithms did not increase with the GC values as the lengths of the time windows went shorter. If we recall the definitions of the F statistics for the average GC and the cumulative GC, the degree-of-freedoms of the distributions of the F statistics are functions of the number of time windows given a time series data. Therefore, the GC value became larger

when the algorithm used shorter time windows, but the corresponding F distribution also changed to require even larger GC value to be significant.

As listed in Table 2, better BIC values were achieved by the average GC and the cumulative GC with time windows similar to the true structure of the simulated data. The result suggested us that the BIC values may be used as an indicator for choosing proper time windows to achieve the best performance, when we use the time windows with equal length in either the average GC or the cumulative GC. However, in many situations, we would prefer to divide the time windows optimally instead of using the time windows with equal lengths. Table 2 also reported the results given by the Opt cumulative GC and the Opt average GC. Compared to the corresponding algorithms with equally divided time windows, the algorithms with optimal time windows gave better TP rates, but the slightly worse FP rates, namely 3% for the Opt cumulative GC and 2% for the Opt average GC on the simulation data. Figure 2B shows that the real change-points for 100 simulations by the proposed BIC-based optimal algorithm were successfully identified for most simulations.

It can be seen that the models with the finer-scale provide us much more accurate results than the static model for the whole time series, and the best performance could be reached when the time windows were divided similar to the underlying true structure of the data. As listed in Table 3, the more time windows we used the longer the time was required for running the algorithm, and the method for optimally dividing the time windows was time consuming. However, in practice, the underlying time-varying structure of the data is unknown. We can either run the optimally dividing algorithm or try different time window lengths and select one optimal time window length by comparing their BIC's.

Test-retest reliability on multiband resting-state data

Here, the reliability of Granger causality can be measured by the correlation between the results inferred for two series of scans upon the same subjects. The Granger

causality was estimated between all directional pairs of the brain regions, and then the Pearson's correlation coefficients were calculated between these causality measurements for the two series scans respectively. For each scan in the multiband test-retest pilot dataset, the Granger causality for each direction was averaged over 17 subjects to give the group Granger causality. The correlations of the group Granger causality between two series of scans demonstrate the reliability of the Granger causality. If the correlations were larger, then reliability might be higher. As shown in Figure 3, the correlations in the group Granger causality between two series of scanning increase monotonically with respect to the number of change-points. A significant correlation ($r = 0.4751$, $p < 0.001$) in the group Granger causality between two series of scanning were observed when the Granger causality was calculated by employing 19 time windows, while the correlation was around 0.3105 in the classical case.

To further demonstrate the effect of the spatial fine-scale details on the Granger causal inference, in 100 randomly selected regions from 1024 ROIs, we compared the correlations established by the voxel-level Granger causality with those by the classic Granger causality, by averaging the time series in the same ROI. The correlation increased from 0.3588 to 0.5125 by calculating the voxel-level Granger causality instead of the classic Granger causality. Furthermore, the combined effects of the temporal and spatial fine-scale details were demonstrated on the test-retest reliability of the Granger causality for 100 regions randomly selected from 1024 ROIs. In Figure 4, the correlation ($r = 0.6059$, $p < 0.001$) between two scans is significantly improved from 0.3588 to 0.6059 by combining the spatial and temporal fine-scale details together.

Monotonicity and significance analyses of Granger causality for the Resting-state fMRI dataset

To verify the theoretic results on the real data set, the Granger causality was estimated by using the time windows with different lengths. In each time series, the first 80 time

points were divided into two sets of time windows, including 8 time windows with 10 time points per window, i.e., a change-point set $S_1 = \{1, 10, 20, 40, 50, 60, 70, 80\}$ and 2 time windows with 40 time points per window, i.e., a change-point set $S_2 = \{1, 40, 80\}$. The cumulative and average Granger causalities with S_1 and S_2 were estimated for all directions between all pairs of brain regions for each subject. The 95% confidence intervals of the differences $D_{j \rightarrow i}^a = F_{j \rightarrow i}^{a, S_1} - F_{j \rightarrow i}^{a, S_2}$ and $D_{j \rightarrow i}^c = F_{j \rightarrow i}^{c, S_1} - F_{j \rightarrow i}^{c, S_2}$ were established for all possible directions $\{i \rightarrow j \mid i, j = 1, 2, \dots, 90 \text{ and } i \neq j\}$. For all directions, the lower bounds of these differences were still larger than 0, which was exactly consistent with our theoretical results. Figure 5B shows that the larger change-point set is used for time-windows dividing, the larger the Granger causality can be achieved.

The results of the average and cumulative Granger causalities are well correlated, as shown in Figure 5A. Actually, if the data are generated by MVAR system that exactly static in each time window, the cumulative Granger causality is larger than the average Granger causality (See Theorem C1 in Appendix C). Under the null hypothesis of non-causality, both Granger causalities approach zeros as the size of data becoming sufficiently large. Moreover, the average Granger causality converges to zero quicker than the cumulative Granger causality (Theorem C2 in Appendix C), i.e., the p -value of significance of the average Granger causality may be smaller, as also shown by the simulation results in the previous section (Table 2) that the average Granger causality performs better than the cumulative Granger causality in terms of detecting non-causality. Therefore, in the following, the average Granger causality was calculated.

As discussed in Appendix B (Corollary B5), some connectivity of Granger causality may be missed if the Granger causality is estimated by the static MVAR model for the whole time series, due to the correlation of the causality measurement and the

time-varying causal coefficients. The correlations between the causality measurement and the sum of the absolute values of the estimated causal coefficients, as well as the absolute value of the sum of the estimated causal coefficients, across all time windows defined by the change-point set (S_1) in the TV-MVAR model were separately studied. For 198 subjects, the absolute value of the median of this summation was plotted against the median of the Granger causality for each direction in Figure 6A. This correlation between average Granger causality and the sum of the causal coefficients decreased for finer time windows, compared with the classic Granger causality. In contrast, this correlation increased, if the absolute value of the median of the sum of the causal coefficients was considered (Figure 6B). As shown in Eq. (A2) in Appendix A, summing the causal coefficients may lead elimination of some positive causal influences with negative ones. In other words, classic Granger causality, or Granger causality with coarser-scale tends to give null prediction when the sum of the causal coefficients is near to zero, but the zero sum may be given by the significant non-zero coefficients with different signs in different time windows.

The results for some particular examples were given in Figure 7. The classic Granger causality using the whole time series data gave near zero¹ causality measurements when the summations of the causal coefficients across all time windows were near to zero for the directions ‘Precuneus_R→Hippocampus_R’ and ‘Thalamus_R→Precuneus_L’. However, both the average Granger causality and the classic Granger causality detected significant causality for the other three directions, as shown in Figure 7, since the sum of the causal coefficients across all time windows were larger than zero.

Granger causality mapping from precuneus of the resting-state fMRI dataset

¹The magnitude of the causality measurement is significantly larger than 0, if the lower bound of the 95% confidence interval of the causality in 198 subjects is greater than 0.0002 for the classical Granger causality and 0.0726 for the average Granger causality.

Now, the approaches were used to identify the Grange causality mapping from the precuneus, which was believed to be the core of many cognitive behaviours and self-conscience and named “mind’s eye” (Cavanna and Trimble, 2006), to other brain regions. The proposed average Granger causality with optimal time-window dividing algorithm (AGC-OTWDA) was used for the resting state dataset by setting the maximum number of time-windows as 3. The significance of a causality influence was detected by the statistical test (See Material and Method). The analysis was also carried out for each subject by the classic Granger causality in contrast.

The classic Granger causality based on the whole time series failed to detect any significant² causal connectivity from the precuneus, while the AGC-OTWDA identified directional neural circuits centred at the precuneus, as shown in Figure 8. Since this data set was collected with the subjects’ eyes open, the information flows from the precuneus and the visual recognition network of brain regions were very significant, which were marked in green in Figure 8.

Results for Attention-Task fMRI dataset

For the attention task, we were to detect the causality between rIPS and rTPJ. The Granger causalities were estimated for all possible pairs of voxels and averaged as the spatial Granger causality. Two ways were used to calculate the Granger causality in this situation. One was to concatenate the time series data in each attention block together into a long time series data, and then compute the Granger causality; the other was to calculate the Granger causality for each attention block and average them, i.e. the average Granger causality defined above. For comparison, we applied these two ways to estimate the Granger causality of two directions, rIPS→rTPJ and rTPJ→rIPS, for 12 subjects.

As shown in Figure 9, the average Granger causality is clearly larger than the classic

²A significant causality is identified if its p -value was less than 0.05 in at least 73% of the subjects.

Granger causality. For both directions, the differences between the causalities established by two different ways were calculated for all 12 subjects and the paired two-sample t-test was done to examine the difference, i.e., average Granger causality subtracting classic Granger causality. The right-tailed t-test suggested that the differences in both directions are significantly larger than 0 with the p -values equal to $6.6482e-006$ for $rIPS \rightarrow rTPJ$ and $9.0040e-005$ for $rTPJ \rightarrow rIPS$, respectively. These results were consistent with our theoretical analysis, i.e. average Granger causality analysis across many shorter time series provided by multi-trials gives larger measurements than one long-term series observation can do.

Conclusions and Discussions

When we have long-term recordings of time series observation, it is important to know how to reliably estimate Granger causality between the time series. A naive and intuitive approach is to take all recordings into the MVAR model to estimate the Granger causality. This approach is based on the widely-accepted statistical belief that the more data are used, the closer the result will be to the true value. However, in this paper, our theoretical analysis and numerical examples demonstrate that this may not be the case. The reliability of the statistical inference depends not only on how much data there is, despite of its importance, but also how finely the model describes the data.

The Granger causality was proved to be equivalent to the transfer information (entropy) between Gaussian processes. It has been widely argued that the definition of the information strongly depends on the modelling configuration for the physical system (Jaynes, 1985). As argued by (Lloyd, 1989), the coarse-grained modelling (such as imperfectly determined evolution) may lead to information loss. Hence, the calculation of Granger causality or transfer information definitely suffers from the issue of the modelling configuration.

In this paper, we have discussed the effects of the fine-scaled details in the MVAR

model on the Granger causality for detecting the directional information flows between time series data and applied the results to fMRI data analysis. This effect is mathematically analysed and we conclude that both the temporal and the spatial characteristics of a MVAR model for the data do affect the reliability of the estimation of Granger causality. A smaller change-point set implies a coarser model and a larger one implies a finer model. As we proved and numerically demonstrated, in the coarser model (with fewer change-points), the Granger causalities including both the cumulative and the average ones are smaller than that in a finer model (with more change-points). In particular, for the dataset generated by the toy model, in the static MVAR model, the regression coefficients are estimated as the (weighted) averages of those estimated by the time-varying MVAR model, so the classic Granger causality becomes the lower bounds (Corollaries B2 and B5). And, the perfect change-point set leads the upper bound, among the information transfer calculations in all TV-MVAR models. Our results demonstrate that the Granger causality depends on the model configuration, thus “the devil is in the details”.

For a given data set, we also try to avoid from using too many change-points for TV-MVAR model to estimate the coefficients properly due to lack of data points in each window. In other words, the larger change-point set implies a finer model (possibly a larger Granger causality) but may become an obstacle for the precise estimation of the Granger causality. Therefore, an optimal change-point set should be a trade-off between the preciseness of statistic estimation and the fineness of modelling. In this paper, we propose a new algorithm for detecting the optimal change-point set based on the Bayesian information criterion (BIC). As illustrated by the data generated by the toy models, this algorithm can precisely identify the change points in the model and increase the reliability and significance for Granger causality detecting. Compared to the models having time windows with equal lengths, the optimal time window dividing algorithm was time consuming. When we focus on the global index measuring the directed information flow instead of the exact evolution course of the underlying structure, the optimal time window can be determined by

either the optimal time window dividing algorithm or by comparing the BIC's given by the models with equally divided time windows in different lengths.

For the real resting-state fMRI data set, as demonstrated by the test-retest reliability analysis, significantly higher reproducibility across two series of scanning on the same subject has been achieved by considering both the temporal and the spatial effects.

We have used the new approach presented in this work to re-visit the Granger causality of brain regions in a few fMRI data sets. For the data set of resting-state fMRI data, the new approach succeeds in detecting a number of Granger causal interdependencies from the precuneus to other brain regions, which cannot be inferred by the classic Granger causality, based on the static MVAR model for the whole BOLD time courses. In particular, a circuit centred at precuneus to the visual network provided a proof of the pivotal role played by precuneus in the visual cognition. In attention-task fMRI data, our approach with spatial-temporal finer-scale details detected the information transfer flows between rIPS and rTPJ.

In conclusion, we have proposed a framework of inferring Granger causality between groups of times series by taking the finer-scale details into the MVAR model. Our approach shows much more power to detect the information transfer between brain regions in fMRI BOLD signals and enhanced the reliability of the estimation. This idea and approach may give rise to a new angle towards the debating of the reliability of applying Granger causality to fMRI data, in particular, resting-state fMRI time courses.

The proposed framework consists of several modules, including the change-points detection, parameter estimation and number of change-points determination. We emphasize that the current algorithm is not the best one since more sophisticated method for each module may improve the overall performance of the analysis. Our

future work will aim to search better algorithms for estimating more precise global Granger causality under the current framework, by using up-to-date approaches in each module and compare with the existing algorithms (Cribben et al., 2012; Havlicek et al., 2010; Hemmelmann et al., 2009; Hesse et al., 2003).

Acknowledgements

JF is a Royal Society Wolfson Research Merit Award holder, partially supported by National Centre for Mathematics and Interdisciplinary Sciences (NCMIS) of the Chinese Academy of Sciences. QL is supported by grant from the National Natural Sciences Foundation of China (No. 11101429) and Research Fund for the Doctoral Program of Higher Education of China (Grant No. 20114307120019). LWL is jointly supported by the Foundation for the Author of National Excellent Doctoral Dissertation of PR China (No. 200921), Shanghai Rising-Star Program (No. 11QA1400400), Shanghai Guidance of Science and Technology (SGST) (No. 09DZ2272900), and also by the Laboratory of Mathematics for Nonlinear Science, Fudan University.

Appendix A: Solution of the time-varying linear regression.

To build up a theoretical analysis of the Granger causality, we assume that the time series are *generated* by the following the first-order (discrete-time) time-varying multivariate auto-regression (TV-MVAR) model:

$$x^{(t+1)} = a_1(t)x^t + b_1(t)y^t + n(t), t = 1, 2, \dots, T, \quad (\text{A1})$$

where n_t is white Gaussian noise statistically independent of x and y :

$$En(t) = 0, \quad E[n(t)n(t')] = \sigma_n^2(t)\delta_{t,t'}.$$

Here, $\delta_{t,t'}$ is the Kronecker delta. Without loss of generality, we can suppose that x^t and y^t are centred, *i.e.*, all means are equal to zeros, and the variances of x^t and y^t both equal to 1, by multiplying coefficients $a_1(t)$ and $b_1(t)$ by their variances,

respectively. Moreover, we assume that the correlation between x^t and y^t are stationary, i.e., $E(x^t y^t) = c$ for a constant $c \in [0, 1]$. Thus, we can perform a simple linear transformation to make x and y orthogonal:

$$z^t = \frac{(y^t - cx^t)}{\sqrt{1-c^2}},$$

which implies that z^t has its mean equal to 0 and its variance equal to 1, and is uncorrelated with x^t . Thus, (A1) becomes:

$$x^{t+1} = \tilde{a}_1(t)x^t + \tilde{b}_1(t)z^t + n^t$$

with $\tilde{a}_1(t) = a_1(t) + b_1(t)c$, $\tilde{b}_1(t) = b_1(t)\sqrt{1-c^2}$. Hence, we can discuss this problem by assuming x^t and y^t are uncorrelated that will not lose generality. Therefore, in the following, we keep assuming x^t and y^t are uncorrelated.

Considering the time-varying linear regression system (A1), we estimate the Granger causality with different time-window split. More generally, we consider (2) or (3) to replace the intrinsic system. To estimate the **theoretical** values of the time-varying Granger causalities by averaging or cumulating as mentioned in the main text, first, we are to estimate the parameters $\bar{a}_1^{S_1}(k)$ and $\bar{b}_1^{(S_1)}(k)$ by minimizing the following residual square errors across the whole time interval:

$$\begin{aligned} & \sum_{t=1}^T E \left[\left(x^{t+1} - \bar{a}_1^{S_1}(k)x^t - \bar{b}_1^{S_1}(k)y^t \right)^2 \right] \\ &= \sum_{t=1}^T E \left\{ \left[\left(a_1(t) - \bar{a}_1^{S_1}(k) \right) x^t + \left(b_1(t) - \bar{b}_1^{S_1}(k) \right) y^t + n^t \right]^2 \right\} \\ &= \sum_{k=1}^m \sum_{t=t_{k-1}}^{t_k-1} E \left\{ \left[\left(a_1(t) - \bar{a}_1^{S_1}(k) \right) x^t + \left(b_1(t) - \bar{b}_1^{S_1}(k) \right) y^t + n^t \right]^2 \right\} \\ &= \sum_{k=1}^m \sum_{t=t_{k-1}}^{t_k-1} \left[\left(a_1(t) - \bar{a}_1^{S_1}(k) \right)^2 + \left(b_1(t) - \bar{b}_1^{S_1}(k) \right)^2 + \sigma_n^2(t) \right] \end{aligned}$$

which is equivalent to a series of minimisation problems:

$$\min_{\bar{a}_1^{S_1}(k)} \sum_{t=t_{k-1}}^{t_k-1} \left(a_1(t) - \bar{a}_1^{S_1}(k) \right)^2, \quad \min_{\bar{b}_1^{S_1}(k)} \sum_{t=t_{k-1}}^{t_k-1} \left(b_1(t) - \bar{b}_1^{S_1}(k) \right)^2$$

for all $k = 1, \dots, m$. It can be seen that the (expectation of) the solution should be

$$\bar{a}_1^{S_1}(k) = \frac{1}{t_k - t_{k-1}} \sum_{t=t_{k-1}}^{t_k-1} a_1(t), \quad \bar{b}_1^{S_1}(k) = \frac{1}{t_k - t_{k-1}} \sum_{t=t_{k-1}}^{t_k-1} b_1(t), \quad \text{for all } k. \quad (\text{A2})$$

Appendix B: Monotonicity of the Ganger causalities of TV-MVAR models

Monotonicity of cumulative Granger causality.

By the estimation of the coefficients, Eq. (A2), the cumulative Granger causality with the given time window lengths can be estimated as:

$$F_{Y \rightarrow X}^{(c, S_1)} = \log \left(\frac{U_{S_1} + \sum_{t=1}^T (b_1(t))^2 + \sum_{t=1}^T \sigma_n^2(t)}{U_{S_1} + V_{S_1} + \sum_{t=1}^T \sigma_n^2(t)} \right),$$

where

$$U_{S_1} = \sum_{k=1}^m \sum_{t=t_{k-1}}^{t_k-1} (a_1(t) - \bar{a}_1^{S_1}(k))^2, \quad V_{S_1} = \sum_{k=1}^m \sum_{t=t_{k-1}}^{t_k-1} (b_1(t) - \bar{b}_1^{S_1}(k))^2.$$

We have the following result.

Theorem B1. For two change-point sets S_1 and S_2 , if $S_1 \subseteq S_2$, then

$$F_{Y \rightarrow X}^{(c, S_1)} \leq F_{Y \rightarrow X}^{(c, S_2)}$$

Proof. Let S_1 be composed of the following integer series:

$$1 = t_0 < t_1 < \dots < t_{m-1} < t_m = T + 1$$

Since the increasing integer series S_2 contains S_1 , we can denote S_2 as follows;

$$1 = (t_0 =) t_1^1 < t_1^2 < \dots < t_1^{n_1} < t_1^{n_1+1} = t_2^1 (= t_1) \\ < \dots < t_{m-1}^{n_{m-1}+1} = t_m^1 (= t_{m-1}) < t_m^2 < \dots < t_m^{n_m} (= t_m) = T + 1.$$

In other words, in each time interval defined by S_1 , for instance, from t_{k-1} to t_k , we

denote $t_k^1 < t_k^2 < \dots < t_k^{n_k} < t_k^{n_k+1}$ as the integers in S_2 , which are located between t_{k-1}

and t_k . For simplicity, we let $t_k^{n_k+1} = t_{k+1}^1$. Then, the TV-MVAR model with respect to

S_2 can be formulated as

$$x^{t+1} = \bar{a}_1^{S_2}(k, q)x^t + \bar{b}_1^{S_2}(k, q)x^t + \tilde{n}(t),$$

$$t_k^q \leq t < t_k^{q+1}, q = 1; \dots; n_k, k = 1; m, \dots \quad (\text{B1})$$

First, we are to prove that $U_{S_1} \geq U_{S_2}$ and $V_{S_1} \geq V_{S_2}$ that are essentially the same. So,

we need to prove one of them, for instance, $V_{S_1} \geq V_{S_2}$.

In fact, we rewrite V_{S_2} as follows:

$$V_{S_2} = \sum_{k=1}^{|S_1|} \sum_{q=1}^{n_k} \sum_{t=t_k^q}^{t_k^{q+1}-1} \left(b_1(t) - \bar{b}_1^{S_2}(\tau(t_k^q)) \right)^2$$

where $\tau(t_k^q)$ denotes the order of t_k^q in the ordered integer set S_2 .

Thus, it is sufficient to show that in each time window of S_1 , it holds that

$$\sum_{t=t_{k-1}}^{t_k-1} \left(b_1(t) - \bar{b}_1^{S_1}(k) \right)^2 \geq \sum_{q=1}^{n_k} \sum_{t=t_k^q}^{t_k^{q+1}-1} \left(b_1(t) - \bar{b}_1^{S_2}(\tau(t_k^q)) \right)^2.$$

We note that

$$\begin{aligned} \sum_{t=t_{k-1}}^{t_k-1} \left(b_1(t) - \bar{b}_1^{S_1}(k) \right)^2 &= \sum_{t=t_{k-1}}^{t_k-1} [b_1(t)]^2 - (t_k - t_{k-1}) [\bar{b}_1^{S_1}(k)]^2, \\ \sum_{q=1}^{n_k} \sum_{t=t_k^q}^{t_k^{q+1}-1} \left(b_1(t) - \bar{b}_1^{S_2}(\tau(t_k^q)) \right)^2 &= \sum_{t=t_{k-1}}^{t_k-1} b_1^2(t) - \sum_{q=1}^{n_k} (t_k^{q+1} - t_k^q) \left(\bar{b}_1^{S_2}(\tau(t_k^q)) \right)^2 \end{aligned}$$

and

$$\bar{b}_1^{S_1}(k) = \frac{1}{t_k - t_{k-1}} \sum_{q=1}^{n_k} (t_k^{q+1} - t_k^q) \bar{b}_1^{S_2}(\tau(t_k^q)), \quad \sum_{q=1}^{n_k} (t_k^{q+1} - t_k^q) = t_k - t_{k-1}.$$

Hence,

$$\begin{aligned} &(t_k - t_{k-1}) [\bar{b}_1^{S_1}(k)]^2 \\ &= (t_k - t_{k-1}) \left[\frac{1}{t_k - t_{k-1}} \sum_{q=1}^{n_k} (t_k^{q+1} - t_k^q) \bar{b}_1^{S_2}(\tau(t_k^q)) \right]^2 \\ &\leq (t_k - t_{k-1}) \frac{1}{t_k - t_{k-1}} \sum_{q=1}^{n_k} (t_k^{q+1} - t_k^q) [\bar{b}_1^{S_2}(\tau(t_k^q))]^2 \\ &= \sum_{q=1}^{n_k} (t_k^{q+1} - t_k^q) [\bar{b}_1^{S_2}(\tau(t_k^q))]^2 \end{aligned} \quad (\text{B2})$$

owing to the well-known fact that the weighted algebraic average is less than the square average with the weighting. This implies $V_{S_1} \geq V_{S_2}$. So, it is with $U_{S_1} \geq U_{S_2}$.

From $V_{S_1} \geq V_{S_2}$, we immediately have

$$\frac{\sum_{t=1}^T (b_1(t))^2 + \sum_{t=1}^T \sigma_n^2(t)}{V_{S_1} + \sum_{t=1}^T \sigma_n^2(t)} \leq \frac{\sum_{t=1}^T (b_1(t))^2 + \sum_{t=1}^T \sigma_n^2(t)}{V_{S_2} + \sum_{t=1}^T \sigma_n^2(t)}$$

Comwindowed by $U_{S_1} \geq U_{S_2}$, we can derive

$$\frac{U_{S_1} + \sum_{t=1}^T (b_1(t))^2 + \sum_{t=1}^T \sigma_n^2(t)}{U_{S_1} + V_{S_1} + \sum_{t=1}^T \sigma_n^2(t)} \leq \frac{U_{S_2} + \sum_{t=1}^T (b_1(t))^2 + \sum_{t=1}^T \sigma_n^2(t)}{U_{S_2} + V_{S_2} + \sum_{t=1}^T \sigma_n^2(t)}$$

This means $F_{Y \rightarrow X}^{(c, S_1)} \leq F_{Y \rightarrow X}^{(c, S_2)}$. From (B2), one can see that the inequality holds if and only if

$$\bar{b}_1^{S_2}(\tau(t_k^q)) = \bar{b}_1^{S_1}(k) \quad (\text{B3})$$

holds for all $q = 1, \dots, n_k$ and all k . □

From Theorem B1 and its proof, in particular Eq. (B3) as the sufficient and necessary condition for $F_{Y \rightarrow X}^{(c, S_1)} = F_{Y \rightarrow X}^{(c, S_2)}$. We immediately have the upper and lower bounds of the cumulative Granger causality.

Corollary B2. Let $S_0 = \{1, T+1\}$ and S_* be the ordered time point set that exactly comprise of the change-points in the TV-MVAR. Then, for any ordered time point set S , we have

$$F_{Y \rightarrow X}^{(c, S_0)} \leq F_{Y \rightarrow X}^{(c, S)} \leq F_{Y \rightarrow X}^{(c, S_*)}$$

This corollary shows that the static (classic) Granger causality actually is the lower-bound of the cumulative Granger causality. And, if the time series are exactly generated by TV-MVAR (A1) with the change-point set S_* , the cumulative Granger causality based on it is the upper bounds of all.

We should point out that Theorem B1 holds under the condition that one switching time set is contained in the other. It does not imply that the more change-points are, the larger cumulative Granger causality it will have.

Conjecture 1. If $|S_2| \geq |S_1|$, then $F_{Y \rightarrow X}^{(c,S_1)} \leq F_{Y \rightarrow X}^{(c,S_2)}$.

We claim that this conjecture is **not true** by a simple counter example. Let $T = 6$, $S_1 = \{1, 4, 7\}$, $S_2 = \{1, 3, 5, 7\}$, and $S = \{1, 7\}$. We suppose that the data is produced by the model (5) with a constant a_1 and $b_1(t)$ is periodic with a period 2, i.e., $b_1(1) = b_1(3) = b_1(5)$ and $b_1(2) = b_1(4) = b_1(6)$. But the two values do not equal pair-wisely. It is clear that for S_2 , the parameters can be estimated as

$$\bar{b}_1^{S_2}(1) = \bar{b}_1^{S_2}(2) = \bar{b}_1^{S_2}(3) = \frac{1}{2}(b_1(1) + b_1(2)),$$

which equals to the whole average

$$\bar{b}_1 = \frac{1}{6}(b_1(1) + b_1(2) + b_1(3) + b_1(4) + b_1(5) + b_1(6)).$$

So, the corresponding Granger Causality with S_2 can be estimated equal to that of the static MVAR model (the change-point is composed of S), i.e., $F_{Y \rightarrow X}^{(c,S_2)} = F_{Y \rightarrow X}^{(c,S)}$.

Noting that $F_{Y \rightarrow X}^{(c,S)} < F_{Y \rightarrow X}^{(c,S_1)}$, where the strict inequality is because of

$$\bar{b}_1^{S_1}(1) = \frac{1}{3}(b_1(1) + b_1(2) + b_1(3)) \neq \bar{b}_1. \quad \text{So, we have } F_{Y \rightarrow X}^{(c,S_2)} < F_{Y \rightarrow X}^{(c,S_1)}$$

despite $|S_2| > |S_1|$. Let us consider a numerical example with $a_1(t) = 1$, $\sigma_n^1(t) = 1$ for all t , and $b_1(1) = b_1(3) = b_1(5) = 1$ and $b_1(2) = b_1(4) = b_1(6) = 0$. Direct calculations lead that

$$\begin{aligned} F_{Y \rightarrow X}^{(c,S_1)} &= \log \left(\frac{\sum_{t=1}^6 (b_1(t))^2 + 6}{\sum_{k=1}^2 \sum_{t=3(k-1)+1}^{3k} (b_1(t) - \bar{b}_1^i(k))^2 + 6} \right) \\ &= \log \frac{6+3}{8/9+6} = \log \frac{81}{62}. \end{aligned}$$

However,

$$\begin{aligned} F_{Y \rightarrow X}^{(c,S_2)} &= \log \left(\frac{\sum_{t=1}^6 (b_1(t))^2 + 6}{\sum_{k=1}^3 \sum_{t=2(k-1)+1}^{2k} (b_1(t) - \bar{b}_1^i(k))^2 + 6} \right) \\ &= \log \frac{6+3}{3/2+6} = \log \frac{6}{5} < \log \frac{81}{62} = F_{Y \rightarrow X}^{(c,S_1)}. \end{aligned}$$

Monotonicity of average Granger causality.

Another approach to estimate the Granger causality of TV-MVAR model is to estimate the Granger causality at each time windows (between switching) can average them according to the length of each time window. Recall $S_1 = \{1 = t_0 < t_1 < \dots < t_{m-1} < t_m = T + 1\}$ as an increasing integer sequence that denote the change-point and the TV-MVAR model as

$$x^{t+1} = \bar{a}_1^{S_1}(k)x^t + \bar{b}_1^{S_1}(k)x^t + \bar{n}(t), t_{k-1} \leq t < t_k, k = \dots m \quad (\text{B4})$$

At each time window, the Granger causality can be estimated as

$$F_{Y \rightarrow X}^{(k, S_1)} = \log \left(\frac{U_k + \sum_{t=t_{k-1}}^{t_k-1} (b_1(t))^2 + \sum_{t=t_{k-1}}^{t_k-1} \sigma_n^2(t)}{U_k + V_k + \sum_{t=t_{k-1}}^{t_k-1} \sigma_n^2(t)} \right)$$

With

$$U_k = \sum_{t=t_{k-1}}^{t_k-1} (a_1(t) - \bar{a}_1^{S_1}(k))^2, V_k = \sum_{t=t_{k-1}}^{t_k-1} (b_1(t) - \bar{b}_1^{S_1}(k))^2.$$

Then, we estimate the Granger Causality by the TV-MVAR model (B4) as follows:

$$F_{Y \rightarrow X}^{(a, S_1)} = \frac{1}{T} \sum_{k=1}^m F_{Y \rightarrow X}^{(k, S_1)}(t_k - t_{k-1}),$$

denoted by the average Granger causality, the weighted average according to the lengths of the time windows. To investigate the relationship of the average Granger causality, we need the following lemma:

Lemma B3. For any positive integer T , any m real constants $[c_t]_{t=1}^T$, any T

nonnegative constants $[p_t]_{t=1}^T$ with $\sum_{t=1}^T p_t = 1$ and any positive constants $[\sigma_t^2]_{t=1}^T$,

we have the following inequality

$$\log \left(\frac{\sum_{t=1}^T c_t^2 p_t + \sigma^2}{\sum_{t=1}^T (c_t - \bar{c})^2 p_t + \sigma^2} \right) \leq \sum_{t=1}^T p_t \log \left(\frac{c_t^2 + \sigma_t^2}{\sigma_t^2} \right)$$

where $\bar{c} = \sum_{t=1}^T p_t c_t$ and $\sigma^2 = \sum_{t=1}^T p_t \sigma_t^2$.

Proof. Let us consider the following function with respect to $C = [c_t]_{t=1}^T$ and

$$\Sigma = \left[\sigma_t^2 \right]_{t=1}^T$$

$$V = \log \frac{\sigma^2 + c^2}{\sigma^2 + v} - \sum_{t=1}^T p_t \log \left(\frac{\sigma_t^2 + c_t^2}{\sigma_t^2} \right)$$

with

$$c^2 = \sum_{t=1}^T c_t^2 p_t, v = \sum_{t=1}^T [c(t) - \bar{c}]^2 p_t = c^2 - (\bar{c})^2.$$

We make minor modifications on the problem according to the following three facts.

First, noting

$$v = \sum_{t=1}^T [c_t - \bar{c}]^2 p_t = \sum_{t=1}^T [c_t]^2 p_t - \left(\sum_{t=1}^T c_t p_t \right)^2 \geq \sum_{t=1}^T |c_t|^2 p_t - \left(\sum_{t=1}^T |c_t| p_t \right)^2,$$

if we replace c_t by $|c_t|$ in V , which is denoted by \hat{V} , then we have $V \leq \hat{V}$.

Therefore, without loss of generality, it is sufficient to prove $\hat{V} \leq 0$ by considering the case that all c_t are nonnegative.

Second, considering

$$\left. \frac{\partial V}{\partial c_t} \right|_{c_t=0} = \frac{2\bar{c}p_t}{\sigma^2 + v},$$

which is positive in the case that there is at least one positive c_t with nonzero p_t .

So, it is sufficient to consider the case that all c_t are positive;

Third, it holds

$$\sum_{t=1}^T p_t \log(\sigma_t^2) \leq \log(\sigma^2)$$

owing to the Jensen's inequality.

In summary, we can consider the following function instead of V :

$$\tilde{V}(y, v, \Sigma) = \log \frac{\sigma^2 + c^2}{\sigma^2 + v} - \sum_{t=1}^T p_t \log \left(\frac{\sigma_t^2 + y_t}{\sigma_t^2} \right).$$

Letting $y_t = (c_t)^2$, owing to the fact that all c_t are nonnegative, $y = [y_t]$, with fixed

c^2 and σ^2 , we are going to show that \tilde{V} is nonnegative by considering the following maximization problem:

$$\begin{aligned} & \max \tilde{V}(y, v, \Sigma) \\ \text{s.t. } & \sum_{t=1}^T y_t p_t = c^2, \sum_{t=1}^T \sqrt{y_t} p_t = \sqrt{c^2 - v}, \sum_{t=1}^T p_t \sigma_t^2 = \sigma^2, \sigma_t^2 > 0, y_t > 0, \forall t \end{aligned} \quad (\text{B5})$$

To solve (B5), we introduce the following auxiliary Lagrange function:

$$\begin{aligned} & L(y, v, \Sigma, \lambda, \mu, \gamma) \\ & = \tilde{V}(y, v, \Sigma) + \lambda \left(\sum_{t=1}^T y_t p_t - c^2 \right) + \mu \left(\sum_{t=1}^T \sqrt{y_t} p_t - \sqrt{c^2 - v} \right) + \gamma \left(\sum_{t=1}^T \sigma_t^2 p_t - \sigma^2 \right) \end{aligned}$$

By the Karush-Kuhn-Tucker conditions, the necessary conditions of the minimum of (B5) include:

$$\begin{aligned} \frac{\partial L}{\partial y_t} &= p_t \left[-\frac{1}{(\sigma_t^2 + y_t)} + \lambda + \frac{\mu}{2\sqrt{y_t}} \right] = 0, \\ \frac{\partial L}{\partial v} &= -\frac{1}{\sigma^2 + v} + \frac{\mu}{2\sqrt{c^2 - v}} = 0, \\ \frac{\partial L}{\partial (\sigma_t^2)} &= p_t \left[-\frac{1}{(\sigma_t^2 + y_t)} + \gamma \right] = 0 \end{aligned}$$

This leads (i) $p_t = 0$ or (ii) $\sigma_t^2 + y_t = 1/\gamma$ and

$$y_t = \left[\frac{\mu}{2(\gamma - \lambda)} \right]^2. \quad (\text{B6})$$

In other words, for these y_t with nonzero p_t , if we are to solve y_t from the above equalities as a function with respect to $\sigma, \lambda, \mu, \gamma, c^2$ and v , which are independent of the index t , then we can only have one expression from (B6). It should be emphasized that we are not solving the values of y_t but its expression with respect to the t -independent quantities, $\sigma, \lambda, \mu, \gamma, c^2$ and v . Therefore, the possible minimum points of $R(y, v)$ only has one single value of y_t . So it is with

$$\sigma_t^2 = \frac{1}{\gamma} - \left[\frac{\mu}{2(\gamma - \lambda)} \right]^2$$

It can be seen that if y_t and σ_t^2 can only have a single value respectively, then $\tilde{V}(y, v, \Sigma) = 0$. So, the maximum of $\tilde{V}(y, v, \Sigma)$ is zero. Hence, the intrinsic V has its maximum equal to zero. Therefore, lemma B2 is proved and the equality holds if and only if y_t and σ_t^2 can only have a single value respectively. \square

Theorem B4. Let S_1 and S_2 be two sequences of increasing integers. If $S_1 \subseteq S_2$, then

$$F_{Y \rightarrow X}^{(a, S_1)} \leq F_{Y \rightarrow X}^{(a, S_2)}.$$

Proof. We denote the sets S_1 and S_2 by the symbols as in the proof of Theorem B1. According to (B1), the Granger causality at the time window of S_2 , the k -th window of S_1 and the q -th can be written as:

$$F_{Y \rightarrow X}^{(k, q, S_2)} = \log \left(\frac{U_{k, q} + \sum_{t=t_k^q}^{t_k^{q+1}-1} (b_1(t))^2 + \sum_{t=t_k^q}^{t_k^{q+1}-1} \sigma_n^2(t)}{U_{k, q} + V_{k, q} + \sum_{t=t_k^q}^{t_k^{q+1}-1} \sigma_n^2(t)} \right)$$

where

$$U_{k, q} = \sum_{t=t_k^q}^{t_k^{q+1}-1} (a_1(t) - \bar{a}_1^{S_2}(\tau(t_k^q)))^2, V_{k, q} = \sum_{t=t_k^q}^{t_k^{q+1}-1} (b_1(t) - \bar{b}_1^{S_2}(\tau(t_k^q)))^2.$$

Then, the average Granger causality with respect to S_2 is

$$F_{Y \rightarrow X}^{(a, S_2)} = \frac{1}{T} \sum_{k=1}^{|S_1|} \sum_{q=1}^{n_k} F_{Y \rightarrow X}^{(k, q, S_2)} (t_k^{q+1} - t_k^q).$$

Note

$$\sum_{q=1}^{n_k} \bar{a}_1^{S_2}(\tau(t_k^q)) (t_k^{q+1} - t_k^q) = \bar{a}_1^{S_1}(k), \sum_{q=1}^{n_k} \bar{b}_1^{S_2}(\tau(t_k^q)) (t_k^{q+1} - t_k^q) = \bar{b}_1^{S_1}(k),$$

and

$$\begin{aligned}\sum_{t=t_k^q}^{t_k^{q+1}-1} [a_1(t)]^2 &= \sum_{t=t_k^q}^{t_k^{q+1}-1} [a_1(t) - \bar{a}_1^{S_2}(\tau(t_k^q))]^2 + [\bar{a}_1^{S_2}(\tau(t_k^q))]^2 (t_k^{q+1} - t_k^q), \\ \sum_{t=t_k^q}^{t_k^{q+1}-1} [b_1(t)]^2 &= \sum_{t=t_k^q}^{t_k^{q+1}-1} [a_1(t) - \bar{b}_1^{S_2}(\tau(t_k^q))]^2 + [\bar{b}_1^{S_2}(\tau(t_k^q))]^2 (t_k^{q+1} - t_k^q).\end{aligned}$$

Compared with $F_{Y \rightarrow X}^{(a, S_2)}$, we can rewrite the term of $F_{Y \rightarrow X}^{(a, S_1)}$, i.e., $F_{Y \rightarrow X}^{(k, S_1)}$, as follows:

$$\begin{aligned}F_{Y \rightarrow X}^{(k, S_1)} &= \log \left(\frac{U_k + \sum_{t=t_{k-1}}^{t_k-1} (b_1(t))^2 + \sum_{t=t_{k-1}}^{t_k-1} \sigma_n^2(t)}{U_k + V_k + \sum_{t=t_{k-1}}^{t_k-1} \sigma_n^2(t)} \right) \\ &= \log \left(\sum_{q=1}^{n_k} [\bar{a}_1^{S_1}(k) - \bar{a}_1^{S_2}(\tau(t_k^q))]^2 (t_k^{q+1} - t_k^q) \right. \\ &\quad \left. + \sum_{q=1}^{n_k} [\bar{b}_1^{S_2}(\tau(t_k^q))]^2 (t_k^{q+1} - t_k^q) + \sum_{q=1}^{n_k} \varepsilon_n^2(q) (t_k^{q+1} - t_k^q) \right) \\ &\quad - \log \left(\sum_{q=1}^{n_k} [\bar{a}_1^{S_1}(k) - \bar{a}_1^{S_2}(\tau(t_k^q))]^2 (t_k^{q+1} - t_k^q) \right. \\ &\quad \left. + \sum_{q=1}^{n_k} [\bar{b}_1^{S_1}(k) - \bar{b}_1^{S_2}(\tau(t_k^q))]^2 (t_k^{q+1} - t_k^q) + \sum_{q=1}^{n_k} \varepsilon_n^2(q) (t_k^{q+1} - t_k^q) \right)\end{aligned}$$

where

$$\varepsilon_n^2(q) = \frac{1}{t_k^{q+1} - t_k^q} \sum_{t=t_k^q}^{t_k^{q+1}-1} \left\{ [a_1(t) - \bar{a}_1^{S_2}(\tau(t_k^q))]^2 + [b_1(t) - \bar{b}_1^{S_2}(\tau(t_k^q))]^2 + \sigma_n^2(t) \right\}.$$

Since

$$\begin{aligned}& \frac{\sum_{q=1}^{n_k} [\bar{a}_1^{S_1}(k) - \bar{a}_1^{S_2}(\tau(t_k^q))]^2 (t_k^{q+1} - t_k^q) + \sum_{q=1}^{n_k} [\bar{b}_1^{S_2}(\tau(t_k^q))]^2 (t_k^{q+1} - t_k^q) + \sum_{q=1}^{n_k} \varepsilon_n^2(q) (t_k^{q+1} - t_k^q)}{\sum_{q=1}^{n_k} [\bar{a}_1^{S_1}(k) - \bar{a}_1^{S_2}(\tau(t_k^q))]^2 (t_k^{q+1} - t_k^q) + \sum_{q=1}^{n_k} [\bar{b}_1^{S_1}(k) - \bar{b}_1^{S_2}(\tau(t_k^q))]^2 (t_k^{q+1} - t_k^q) + \sum_{q=1}^{n_k} \varepsilon_n^2(q) (t_k^{q+1} - t_k^q)} \\ & \leq \frac{\sum_{q=1}^{n_k} [\bar{b}_1^{S_2}(\tau(t_k^q))]^2 (t_k^{q+1} - t_k^q) + \sum_{q=1}^{n_k} \varepsilon_n^2(q) (t_k^{q+1} - t_k^q)}{\sum_{q=1}^{n_k} [\bar{b}_1^{S_1}(k) - \bar{b}_1^{S_2}(\tau(t_k^q))]^2 (t_k^{q+1} - t_k^q) + \sum_{q=1}^{n_k} \varepsilon_n^2(q) (t_k^{q+1} - t_k^q)}\end{aligned}$$

Theorem B3 can be derived by directly employing Lemma B3. In addition, the inequality holds if and only if $\bar{b}_1^{S_2}(\tau(t_k^q))$ and $\varepsilon_n^2(q)$ can only pick values independent of the index q (but possibly depending on the index k), respectively. \square

Similar to Corollary B2, from Theorem B4 and its proof, in particular the sufficient

and necessary condition for $F_{Y \rightarrow X}^{(a, S_1)} = F_{Y \rightarrow X}^{(a, S_2)}$. We immediately have the upper and lower bounds of the cumulative Granger causality.

Corollary B5. Let $S_0 = \{1, T+1\}$ and S_* be the ordered time point set that exactly comprise of the change-points in the TV-MVAR model. Then, for any ordered time point set S , we have

$$F_{Y \rightarrow X}^{(a, S_0)} \leq F_{Y \rightarrow X}^{(a, S)} \leq F_{Y \rightarrow X}^{(a, S_*)}.$$

This corollary shows that the static (classic) Granger causality actually is the lower-bound of the average Granger causality. And, if the time series are exactly generated by TV-MVAR (A1) with the change-point set S_* , the average Granger causality based on it is the upper bounds of all.

We should also emphasize that the following conjecture is *not true*.

Conjecture B2. If $|S_2| \geq |S_1|$, then $F_{Y \rightarrow X}^{(a, S_1)} \leq F_{Y \rightarrow X}^{(a, S_2)}$.

That is to say, the average Granger causality is monotonic with respect to the containing relation between the change-point set, but not monotonic with respect to the size of the change-point sets. A counter-example can be easily established by the same way as in Remark 1.

Appendix C: Comparison between cumulative and average Ganger causalities

Magnitude comparison.

Actually, the two sorts of Granger causalities of the TV-MVAR model do not have definite magnitude relation. First, we show in the following theorem, the relation that cumulative Granger causality is greater than the average Granger causality with the same change-point set is **conditional**.

Theorem C1. Let S be a sequence of increasing integers. If the following quantity

$$\frac{1}{t_k - t_{k-1}} \left[\sum_{t=t_{k-1}}^{t_k-1} (a_1(t) - \bar{a}_1(k))^2 + \sum_{t=t_{k-1}}^{t_k-1} (b_1(t) - \bar{b}_1(k))^2 + \sum_{t=t_{k-1}}^{t_k-1} \sigma_n^2(t) \right]$$

With

$$\bar{a}_1(k) = \frac{1}{t_k - t_{k-1}} \sum_{t=t_{k-1}}^{t_k-1} a_1(t), \bar{b}_1(k) = \frac{1}{t_k - t_{k-1}} \sum_{t=t_{k-1}}^{t_k-1} b_1(t)$$

is independent of the index k , then

$$F_{Y \rightarrow X}^{(a,S)} \leq F_{Y \rightarrow X}^{(c,S)}.$$

Proof. Let $S = \{1 = t_0 < t_1 < \dots < t_{m-1} < t_m = T + 1\}$. And, with the same notations we used above, we have

$$F_{Y \rightarrow X}^{(c,S)} = \log \left(\frac{\sum_{k=1}^m \sum_{t=t_{k-1}}^{t_k-1} (a_1(t) - \bar{a}_1(k))^2 + \sum_{t=1}^T (b_1(t))^2 + \sum_{t=1}^T \sigma_n^2(t)}{\sum_{k=1}^m \sum_{t=t_{k-1}}^{t_k-1} (a_1(t) - \bar{a}_1(k))^2 + \sum_{k=1}^m \sum_{t=t_{k-1}}^{t_k-1} (b_1(t) - \bar{b}_1(k))^2 + \sum_{t=1}^T \sigma_n^2(t)} \right),$$

and

$$F_{Y \rightarrow X}^{(a,S)} = \frac{1}{T} \sum_{k=1}^m (t_k - t_{k-1}) \log \left(\frac{\sum_{t=t_{k-1}}^{t_k-1} (a_1(t) - \bar{a}_1(k))^2 + \sum_{t=t_{k-1}}^{t_k-1} (b_1(t))^2 + \sum_{t=t_{k-1}}^{t_k-1} \sigma_n^2(t)}{\sum_{t=t_{k-1}}^{t_k-1} (a_1(t) - \bar{a}_1(k))^2 + \sum_{t=t_{k-1}}^{t_k-1} (b_1(t) - \bar{b}_1(k))^2 + \sum_{t=t_{k-1}}^{t_k-1} \sigma_n^2(t)} \right)$$

Let $\bar{b}_1 = \frac{1}{T} \sum_{t=1}^T b_1(t)$. Thus, we can rewrite them as

$$F_{Y \rightarrow X}^{(c,S)} = \log \left(\frac{\sum_{k=1}^m \sum_{t=t_{k-1}}^{t_k-1} (a_1(t) - \bar{a}_1(k))^2 + \sum_{t=1}^m (\bar{b}_1(k))^2 (t_k - t_{k-1}) + \sum_{t=1}^m \sum_{t=t_{k-1}}^{t_k-1} (b_1(t) - \bar{b}_1(k))^2 + \sum_{t=1}^T \sigma_n^2(t)}{\sum_{k=1}^m \sum_{t=t_{k-1}}^{t_k-1} (a_1(t) - \bar{a}_1(k))^2 + \sum_{k=1}^m \sum_{t=t_{k-1}}^{t_k-1} (b_1(t) - \bar{b}_1(k))^2 + \sum_{t=1}^T \sigma_n^2(t)} \right)$$

and

$$F_{Y \rightarrow X}^{(a,S)} = \frac{1}{T} \sum_{k=1}^m (t_k - t_{k-1}) \times \log \left(\frac{\sum_{t=t_{k-1}}^{t_k-1} (a_1(t) - \bar{a}_1(k))^2 + \sum_{t=t_{k-1}}^{t_k-1} (b_1(t) - \bar{b}_1(k))^2 + (\bar{b}_1(k))^2 (t_k - t_{k-1}) + \sum_{t=t_{k-1}}^{t_k-1} \sigma_n^2(t)}{\sum_{t=t_{k-1}}^{t_k-1} (a_1(t) - \bar{a}_1(k))^2 + \sum_{t=t_{k-1}}^{t_k-1} (b_1(t) - \bar{b}_1(k))^2 + \sum_{t=t_{k-1}}^{t_k-1} \sigma_n^2(t)} \right).$$

In addition, letting

$$\theta_k = \frac{1}{t_k - t_{k-1}} \left[\sum_{t=t_{k-1}}^{t_k-1} (a_1(t) - \bar{a}_1(k))^2 + \sum_{t=t_{k-1}}^{t_k-1} (b_1(t) - \bar{b}_1(k))^2 + \sum_{t=t_{k-1}}^{t_k-1} \sigma_n^2(t) \right],$$

$$\alpha_k = \frac{1}{t_k - t_{k-1}} \sum_{t=t_{k-1}}^{t_k-1} (\bar{b}_1(k))^2, p_k = \frac{(t_k - t_{k-1})}{T}$$

due to the condition, θ_k is independent of k , which is denoted by θ . Thus, we have

$$F_{Y \rightarrow X}^{(c,S)} = \log \left(\frac{\sum_{k=1}^m \alpha_k p_k + \sum_{k=1}^m \theta_k p_k}{\sum_{k=1}^m \theta_k p_k} \right) = \log \left(\frac{\sum_{k=1}^m \alpha_k p_k + \theta}{\theta} \right),$$

and

$$F_{Y \rightarrow X}^{(a,S)} = \sum_{k=1}^m p_k \log \left(\frac{\alpha_k + \theta_k}{\theta_k} \right) = \sum_{k=1}^m p_k \log \left(\frac{\alpha_k + \theta}{\theta} \right).$$

Thus, we can conclude $F_{Y \rightarrow X}^{(a,S)} \leq F_{Y \rightarrow X}^{(c,S)}$, owing to the Jensen's inequality. This completes the proof. \square

From Theorem C1, if the TV-MVAR system is time-varying with the segments well known, which implies that at each time window, the system is static, we can conclude that the average Grange causality is smaller than the cumulative Granger causality.

On the other hand, if the condition in Theorem C1 is not satisfied, then it will not be surprising that $F_{Y \rightarrow X}^{(a,S)} > F_{Y \rightarrow X}^{(c,S)}$ holds. Here is a counter-example. A special situation is to solve the time-varying regression model (A1) as a static one, i.e., taking all time points as the change-point set, i.e., $S = \{1, \dots, T+1\}$. By a proper transformation, we can still let the variances of y and x equal to 1 for all time. Let $a_1(t) = 0$ for all t . But the variance of the noise may be time-varying. The defined Granger causalities become:

$$F_{Y \rightarrow X}^S = \log \left(\frac{\frac{1}{T} \sum_{t=1}^T \sigma_n^2(t) + \frac{1}{T} \sum_{t=1}^T [b_1(t)]^2}{\frac{1}{T} \sum_{t=1}^T \sigma_n^2(t)} \right), \hat{F}_{Y \rightarrow X}^S = \frac{1}{T} \sum_{t=1}^T \log \left(\frac{\sigma_n^2(t) + [b_1(t)]^2}{\sigma_n^2(t)} \right).$$

Pick $T = 3, b_1 = 1, b_2 = \sqrt{2}, b_3 = \sqrt{3}, \sigma_1 = \sqrt{3}, \sigma_2 = \sqrt{2}, \sigma_3 = 1$. Then,

$$F_{Y \rightarrow X} = \log 2 < \hat{F}_{Y \rightarrow X} = \frac{1}{3} \left[\log \left(\frac{4}{3} \right) + \log(2) + \log(4) \right].$$

Comparison between the asymptotic square moments under null hypothesis.

For simplicity, we suppose that the time-varying system (A1) is a switching system with equal-length time windows and the segment points are exactly known. The general case will be treated in our future paper. Thus, (A1) becomes a series of static linear system as follows:

$$x^{t+1} = \bar{a}_1(k)x^t + \bar{b}_1(k)y^t + n(t), t_k \leq t < t_{k+1}, k = 1, 2, \dots, m, \quad (C1)$$

Here, $t_{k+1} - t_k = \frac{n}{m}$ for all k . Under the null hypothesis, namely, the coefficients

$b_1(t) = 0$ hold for all t , (C1) becomes

$$x^{t+1} = \bar{a}_1(k)x^t + \tilde{n}(t), t_k \leq t < t_{k+1}, k = 1, 2, \dots, m. \quad (C2)$$

Their residual squared errors at each time window are

$$RSS_1(k) = \sum_{t=t_k}^{t_{k+1}-1} n^2(t) \quad \text{and} \quad RSS_0(k) = \sum_{t=t_k}^{t_{k+1}-1} \tilde{n}^2(t).$$

Then, the CGS and AGC can be formulated as follows respectively:

$$F_{Y \rightarrow X}^c = \log \left(\frac{\sum_{k=1}^m RSS_0(k)}{\sum_{k=1}^m RSS_1(k)} \right) = \log \left(1 + \frac{\sum_{k=1}^m [RSS_0(k) - RSS_1(k)]}{\sum_{k=1}^m RSS_1(k)} \right) \sim \frac{\sum_{k=1}^m [RSS_0(k) - RSS_1(k)]}{\sum_{k=1}^m RSS_1(k)}$$

$$F_{Y \rightarrow X}^a = \frac{1}{m} \sum_{k=1}^m \log \left(\frac{RSS_0(k)}{RSS_1(k)} \right) = \frac{1}{m} \sum_{k=1}^m \log \left(1 + \frac{RSS_0(k) - RSS_1(k)}{RSS_1(k)} \right) \sim \frac{1}{m} \sum_{k=1}^m \frac{RSS_0(k) - RSS_1(k)}{RSS_1(k)}$$

as n goes to infinity. Therefore, the cumulative Granger causality converges the following in distribution:

$$F_{Y \rightarrow X}^c \times \frac{n-2m-1}{m} \approx \frac{\sum_{k=1}^m [RSS_0(k) - RSS_1(k)]}{\sum_{k=1}^m RSS_1(k)} \times \frac{n-2m-1}{m} \sim F(m, n-2m-1)$$

and the average Granger causality converges to:

$$F_{Y \rightarrow X}^a \times \frac{n/m-3}{1} \approx \frac{1}{m} \sum_{k=1}^m \frac{RSS_0(k) - RSS_1(k)}{RSS_1(k)} \times \frac{n/m-3}{1}$$

with each

$$\frac{RSS_0(k) - RSS_1(k)}{RSS_1(k)} \times \frac{n/m-3}{1} \sim F(1, \frac{n}{m}-3)$$

So, their asymptotic expectations are

$$E(F_{Y \rightarrow X}^c) \approx \frac{m}{n-2m-1} \frac{n-2m-1}{n-2m-3} = \frac{1}{\frac{n}{m}-2-\frac{3}{m}}, E(F_{Y \rightarrow X}^a) \approx \frac{\frac{n}{m}-3}{\frac{n}{m}-5} \frac{1}{\frac{n}{m}-3} = \frac{1}{\frac{n}{m}-5},$$

as $n \rightarrow \infty$.

The dominant converge rates are same, equivalently $\frac{m}{n}$. Then, let us take a look at

their asymptotic square moments. By the square moment of the F -distribution and simple algebras, we have

$$E\left\{\left[F_{Y \rightarrow X}^c\right]^2\right\} \approx \left(1 + \frac{2}{m}\right) \left(\frac{m}{n}\right)^2.$$

As for the AGC, with $f_k = \frac{RSS_0(k) - RSS_1(k)}{RSS_1(k)} \sim F\left(1, \frac{n}{m} - 3\right)$, we have

$$E\left\{\left[F_{Y \rightarrow X}^a\right]^2\right\} \cong \left(\frac{1}{n/m - 3}\right)^2 E\left\{\frac{1}{m} \sum_{k=1}^m f_k\right\}^2 \leq \left(\frac{1}{n/m - 3}\right)^2 \left(\frac{1}{m}\right) \sum_{k=1}^m E\{f_k\}^2$$

With

$$E\{f_k^2\} \cong 3 \left(\frac{\frac{n}{m} - 3}{\frac{n}{m} - 5}\right)^2,$$

which implies

$$E\left\{\left[F_{Y \rightarrow X}^a\right]^2\right\} < \frac{3}{m} \left(\frac{m}{n}\right)^2$$

holds in the asymptotic sense, i.e, if n is a sufficiently large. Therefore, in the asymptotic squared meaning, for $m > 1$, we have

$$E\left\{\left[F_{Y \rightarrow X}^a\right]^2\right\} < E\left\{\left[F_{Y \rightarrow X}^c\right]^2\right\}$$

asymptotically. In other words, the average Granger causality converges to zero more quickly than the cumulative Granger causality.

Theorem C2. Under the setup as mentioned above, $\limsup_{n \rightarrow \infty} \frac{E\left\{\left[F_{Y \rightarrow X}^a\right]^2\right\}}{E\left\{\left[F_{Y \rightarrow X}^c\right]^2\right\}} < 1$ for

$m > 1$.

And, the larger m is, the higher asymptotic converge rate the average Granger causality is than the cumulative one. □

References

Ahmed, A., Xing, E., 2009. Recovering time-varying networks of dependencies in social and biological studies. *Proceedings of the National Academy of Sciences* 106, 11878-11883.

Biswal, B., Mennes, M., Zuo, X.-N., et.al., 2010. Toward discovery science of human brain function. *Proceedings of the National Academy of Sciences* 107, 4734-4739.

Cavanna, A.E., Trimble, M.R., 2006. The precuneus: a review of its functional anatomy and behavioural correlates. *Brain*. 129, 564-583. Epub 2006 Jan 2006.

Chen, M.-p., Lee, C.-C., Hsu, Y.-C., 2011. The impact of American depositary receipts on the Japanese index: Do industry effect and size effect matter? *Economic Modelling* 28, 526-539.

Cribben, I., Haraldsdottir, R., Atlas, L.Y., Wager, T.D., Lindquist, M.A., 2012. Dynamic connectivity regression: determining state-related changes in brain connectivity. *Neuroimage*. 61, 907-920.

Deshpande, G., Sathian, K., Hu, X., 2010. Effect of hemodynamic variability on Granger causality analysis of fMRI. *NeuroImage* 52, 884-896.

Ding, M., Bressler, S.L., Yang, W., Liang, H., 2000. Short-window spectral analysis of cortical event-related potentials by adaptive multivariate autoregressive modeling: data preprocessing, model validation, and variability assessment. *Biological Cybernetics* 83, 35-45.

Evan, K., Snigdhanu, C., Auroop R., G., 2011. Exploring Granger causality between global average observed time series of carbon dioxide and temperature. *Theoretical and Applied Climatology* 104, 325-335.

Friston, K.J., Frith, C.D., Turner, R., Frackowiak, R.S., 1995. Characterizing evoked hemodynamics with fMRI. *Neuroimage*. 2, 157-165.

Ge, T., Feng, J., Grabenhorst, F., Rolls, E., 2012. Componential Granger causality, and its application to identifying the source and mechanisms of the top-down biased activation that controls attention to affective vs sensory processing. *NeuroImage* 59, 1846-1858.

Ge, T., Kendrick, K., Feng, J., 2009. A Novel Extended Granger Causal Model Approach Demonstrates Brain Hemispheric Differences during Face Recognition Learning. *PLoS Comput Biol* 5, e1000570.

Granger, C.W.J., 1969. Investigating Causal Relations by Econometric Models and Cross-spectral Methods. *Econometrica* 37, 424-438.

Guo, S., Wu, J., Ding, M., Feng, J., 2008. Uncovering Interactions in the Frequency Domain. *PLoS Comput Biol* 4, e1000087.

Havlicek, M., Jan, J., Brazdil, M., Calhoun, V.D., 2010. Dynamic Granger causality based on Kalman filter for evaluation of functional network connectivity in fMRI data. *Neuroimage*. 53, 65-77.

Hemmelmann, D., Ungureanu, M., Hesse, W., Wustenberg, T., Reichenbach, J.R., Witte, O.W., Witte, H., Leistriz, L., 2009. Modelling and analysis of time-variant directed interrelations between brain regions based on BOLD-signals. *Neuroimage*. 45, 722-737.

Hesse, W., Moller, E., Arnold, M., Schack, B., 2003. The use of time-variant EEG Granger causality for inspecting directed interdependencies of neural assemblies. *Journal of Neuroscience Methods* 124, 27-44.

Jaynes, E.T., 1985. Some random observations. *Synthese* 63, 115-138.

Lloyd, S., 1989. Use of mutual information to decrease entropy: implications for the second law of thermodynamics. *Physical Review A* 39, 5378-5386.

Luo, Q., Ge, T., Feng, J., 2011. Granger causality with signal-dependent noise. *NeuroImage* 57, 1422-1429.

Luscombe, N.M., Madan Babu, M., Yu, H., Snyder, M., Teichmann, S.A., Gerstein, M., 2004. Genomic analysis of regulatory network dynamics reveals large topological changes. *Nature* 431, 308-312.

Ohiorhenuan, I.E., Mechler, F., Purpura, K.P., Schmid, A.M., Hu, Q., Victor, J.D., 2010. Sparse coding and high-order correlations in fine-scale cortical networks. *Nature* 466, 617-621.

- Psaradakis, Z., Ravn, M.O., Sola, M., 2005. Markov switching causality and the money–output relationship. *Journal of Applied Econometrics* 20, 665-683.
- Sato, J.o.R., Junior, E.A., Takahashi, D.Y., de Maria Felix, M., Brammer, M.J., Morettin, P.A., 2006. A method to produce evolving functional connectivity maps during the course of an fMRI experiment using wavelet-based time-varying Granger causality. *Neuroimage* 31, 187-196.
- Schippers, M., Renken, R., Keysers, C., 2011. The effect of intra- and inter-subject variability of hemodynamic responses on group level Granger causality analyses. *NeuroImage* 57, 22-36.
- Smerieri, A., Rolls, E.T., Feng, J., 2010. Decision Time, Slow Inhibition, and Theta Rhythm. *The Journal of neuroscience* 30, 14173-14181.
- Smith, S.M., Bandettini, P.A., Miller, K.L., Behrens, T.E., Friston, K.J., David, O., Liu, T., Woolrich, M.W., Nichols, T.E., 2012. The danger of systematic bias in group-level FMRI-lag-based causality estimation. *NeuroImage* 59, 1228-1229.
- Smith, S.M., Miller, K.L., Salimi-khorshidi, G., Webster, M., Beckmann, C.F., Nichols, T.E., Ramsey, J.D., Woolrich, M.W., 2011. Network modelling methods for FMRI. *NeuroImage* 54, 875-891.
- Sommerlade, L., Thiel, M., Platt, B., Plano, A., Riedel, G., Grebogi, C., Timmer, J., Schelter, B., 2012. Inference of Granger causal time-dependent influences in noisy multivariate time series. *J Neurosci Methods* 203, 173-185.
- Tunçbag, N., Kar, G., Gursoy, A., Keskin, O., Nussinov, R., 2009. Towards inferring time dimensionality in protein-protein interaction networks by integrating structures: the p53 example. *Mol. BioSyst.* 5, 1770-1778.
- Tzourio-Mazoyer, N., Landeau, B., Papathanassiou, D., Crivello, F., Etard, O., Delcroix, N., Mazoyer, B., Joliot, M., 2002. Automated anatomical labeling of activations in SPM using a macroscopic anatomical parcellation of the MNI MRI single-subject brain. *Neuroimage.* 15, 273-289.
- Warne, A., 2000. Causality and Regime Inference in a Markov Switching VAR. Sveriges Riksbank (Central Bank of Sweden).
- Wen, X., Yao, L., Liu, Y., Ding, M., 2012. Causal interactions in attention networks predict behavioral performance. *The Journal of neuroscience* 32, 1284-1292.
- Wiener, N., 1956. *The Theory of Prediction*. In: BeckenBach, E. (Ed.), *Modern mathematics for the engineer*. McGraw-Hill, New York, pp. 165 - 190.
- Yan, C., Zang, Y., 2010. DPARSF: a MATLAB toolbox for "pipeline" data analysis of resting-state fMRI. *Frontiers in Systems Neuroscience* 4.
- Zalesky, A., Fornito, A., Harding, I.H., Cocchi, L., Yucel, M., Pantelis, C., Bullmore, E.T., 2010. Whole-brain anatomical networks: does the choice of nodes matter? *NeuroImage* 50, 970-983.
- Zhu, J., Chen, Y., Leonardson, A.S., Wang, K., Lamb, J.R., Emilsson, V., Schadt, E.E., 2010. Characterizing Dynamic Changes in the Human Blood Transcriptional Network. *PLoS Comput Biol* 6, e1000671.

Tables and Figure Captions

Table 1. The 95% confidence intervals of the differences between the cumulative causality measurements established from time windows with different lengths.

direction	$X \rightarrow Y$		$Y \rightarrow X$	
quantile	0.025 th	0.975 th	0.025 th	0.975 th
D_1^a	0.0078	0.0321	0.0053	0.0341
D_2^a	0.0085	0.0448	0.0109	0.0453
D_3^a	0.0002	0.0128	0.0003	0.0229
D_1^c	0.0078	0.0285	0.0055	0.0333
D_2^c	0.0105	0.0437	0.0116	0.0480
D_3^c	0.0002	0.0156	0.0003	0.0264

Table 2. Performance comparison for different methods. ‘Classical GC’ is short for the classic Granger causality. ‘Cumulative GC’ is the cumulative Granger causality. ‘Average GC’ is the average Granger causality. ‘opt Cumulative GC’ stands for the cumulative Granger causality with optimally divided time windows, and ‘opt Average GC’ means the average Granger causality with optimally determined time windows. $\bar{F}_{X \rightarrow Y}$ and $\bar{F}_{Y \rightarrow X}$ are the average values of the Granger causality measurements over 100 simulations, and \overline{BIC} is the mean value of the BIC for 100 simulations. The threshold for significance is 1e-11.

Method	Window Length	TP	FP	TN	FN	$\bar{F}_{X \rightarrow Y}$	$\bar{F}_{Y \rightarrow X}$	\overline{BIC}
Classical GC	1200	0%	0%	100%	100%	0.0023	0.0007	6.9489
Cumulative GC	10	50%	0%	100%	50%	0.2484	0.1331	8.5869
	50	72%	0%	100%	28%	0.1303	0.0208	7.2041
	100	75%	0%	100%	25%	0.1177	0.0101	7.0188
	300	70%	0%	100%	30%	0.0709	0.0032	6.9417
	600	0%	0%	100%	100%	0.0071	0.0015	6.9819
Average GC	10	39%	0%	100%	61%	0.2620	0.1516	8.5869

	50	85%	0%	100%	15%	0.1219	0.0212	7.2041
	100	93%	0%	100%	7%	0.1094	0.0102	7.0188
	300	92%	0%	100%	8%	0.0681	0.0032	6.9417
	600	14%	0%	100%	86%	0.0074	0.0015	6.9819
Opt Cumulative GC		90%	3%	97%	10%	0.1320	0.0131	6.8780
Opt Average GC		94%	2%	98%	6%	0.1453	0.0080	6.8780

Table 3. Comparison of running time (in second) for different methods. The classic Granger causality treated the whole time series as one time window. The average Granger causality and the cumulative Granger causality were applied to the data by dividing the time series into equally time windows with different lengths. The average Granger causality and the cumulative Granger causality had also been used after optimally dividing the time windows by the proposed algorithm. This simulation was carried out by a computer with Intel® Core™ 2 CPU T5600 @ 1.83GHz, 1.83GHz, and 1.5G RAM.

	One time window	Time windows with equal length					Optimally divided time windows
Window length	1200	600	300	100	50	10	
Running time	0.0073	0.2936	0.4697	0.9969	1.9747	9.8709	346.5863

Figure 1. Monotonicity of the cumulative Granger causality and the average Granger causality respectively. If we consider finer time windows with the same length, the change-point set can be derived from the window length, so the causality established by different change-point sets can be equivalently denoted by the corresponding window lengths m_i for S_i .

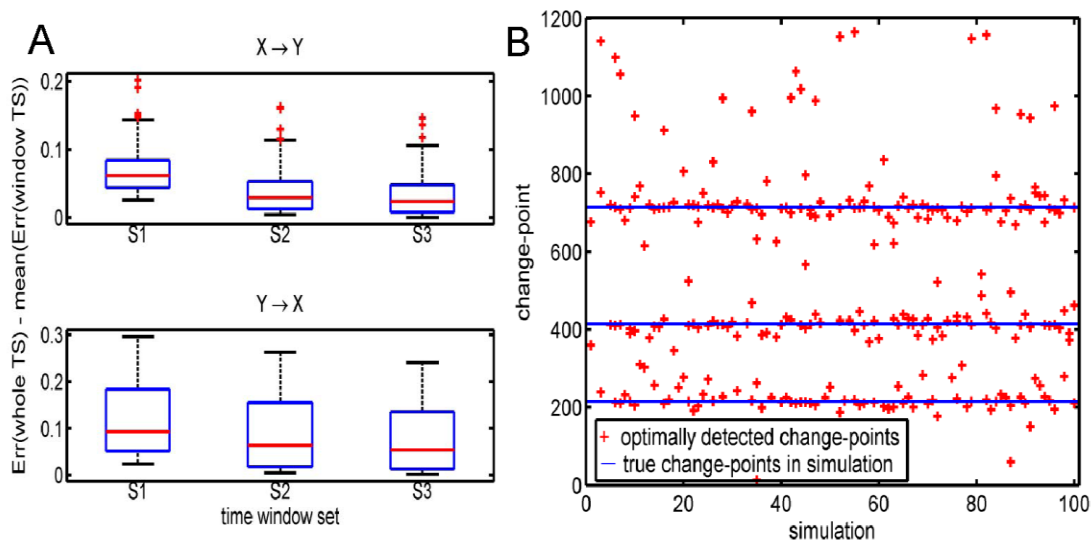


Figure 2. Results for simulation model: (A) Residual variance comparison between the models established from the whole time series and those models fitted on different time window sets. (B) Optimally detected change-points for 100 simulations.

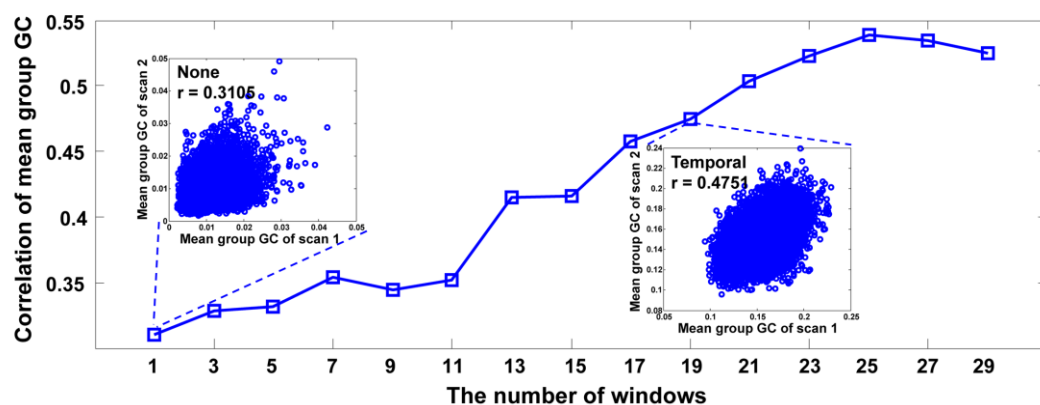


Figure 3. Correlation of the mean group Granger causalities (GC) between two series of scanning upon the same subject set versus the number of time windows for the average Granger causality. The inset plots show the correlation between two scans of selected the number of windows, in which each circle represents the GC between two

ROIs parcellated by AAL atlas.

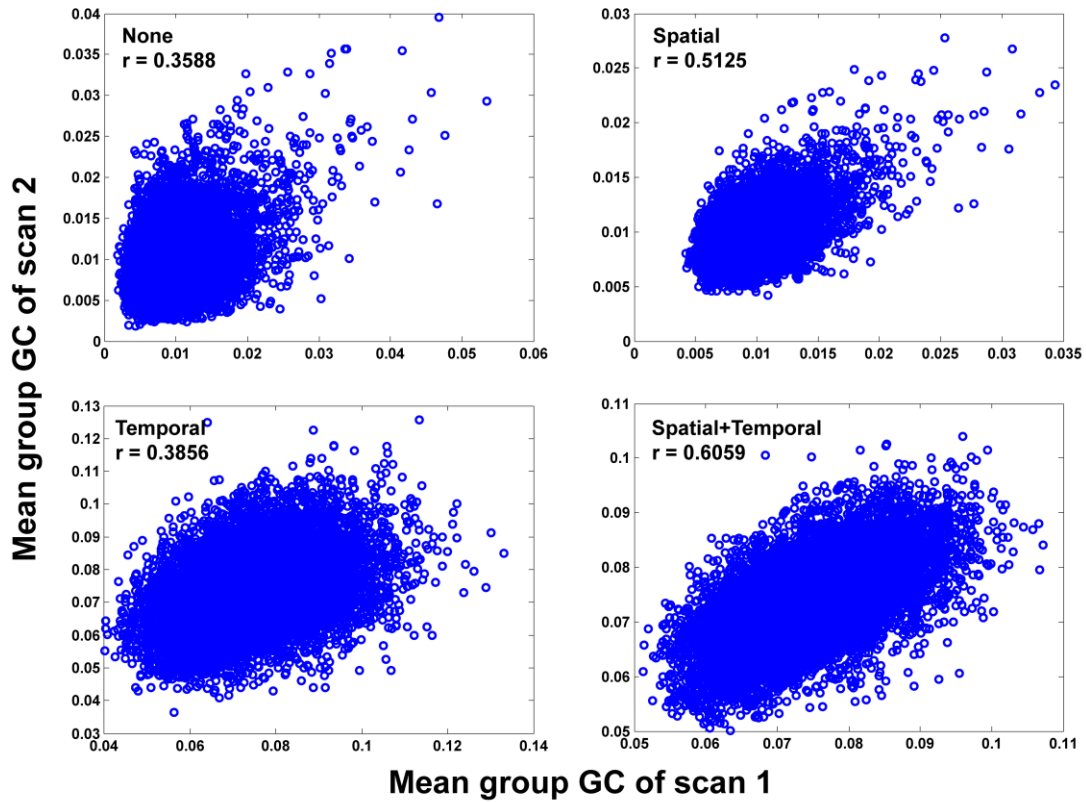


Figure 4. Correlation between the Granger causality between two series of scanning upon the same subject set. The causality measurements were calculated by different methods: (A) the traditional Granger causality; (B) the voxel level Granger causality; (C) the average Granger causality; (D) the spatial-temporal Granger causality.

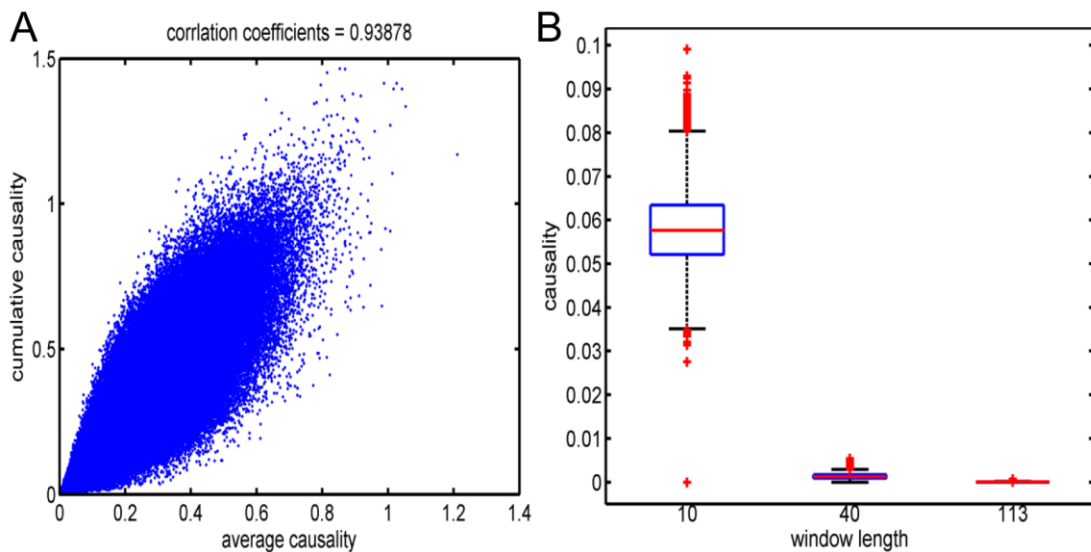


Figure 5. Granger causality results of the resting-state data set. (A) Average Granger

causality versus cumulative Granger causality on the resting state data set. (B) Comparison of the average Granger causality established by different time window lengths.

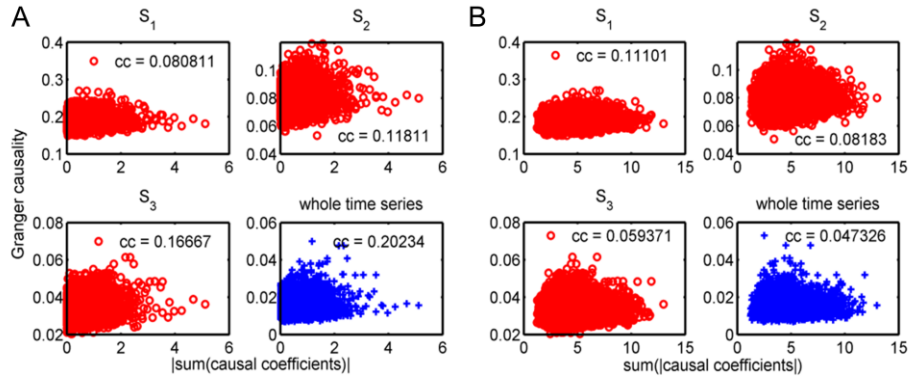


Figure 6. Granger causality versus the sum of the causal coefficients across time windows. The causal coefficients were estimated for each time window defined by S_1 for each subject. The medians of the causality among 198 subjects were established by different change-point sets, including S_1, S_2, S_3 and the whole time series without change-point (specified as the titles for subplots in the figure). Different change-point sets gave different Granger causality value, since the Granger causality value increased as the time window lengths decrease. (A) Correlation to the absolute value of the median of the sum of the causal coefficients over all time windows; (B) Correlation to the median of the sum of the absolute value of the causal coefficients over all time windows. The p -values for all correlations are below the significant threshold.

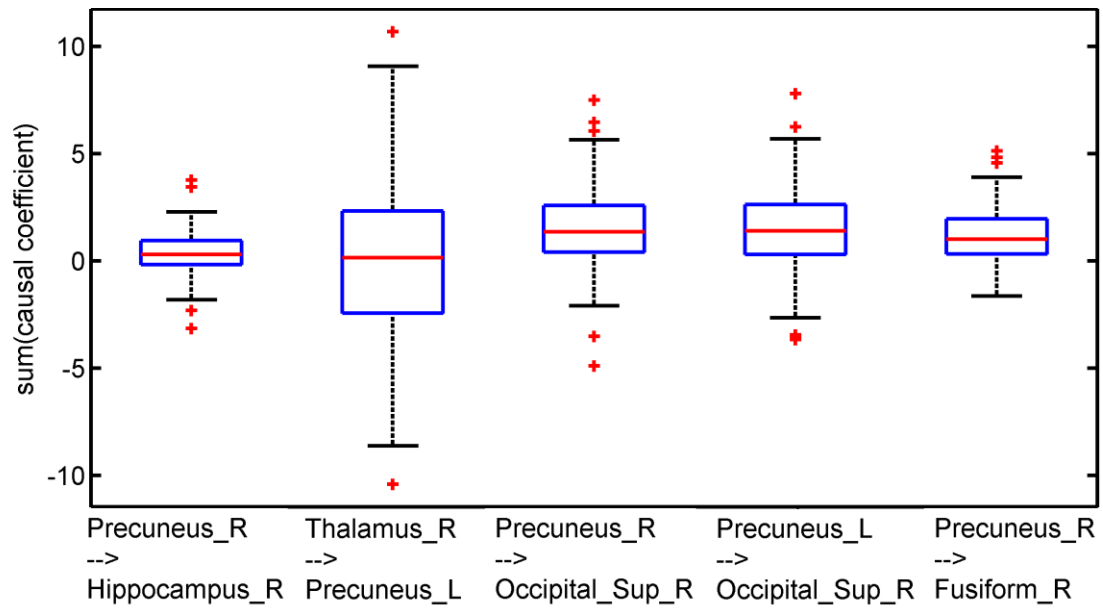


Figure 7. Boxplot for sum of the causal coefficients across all time windows of the change-point set S_1 .

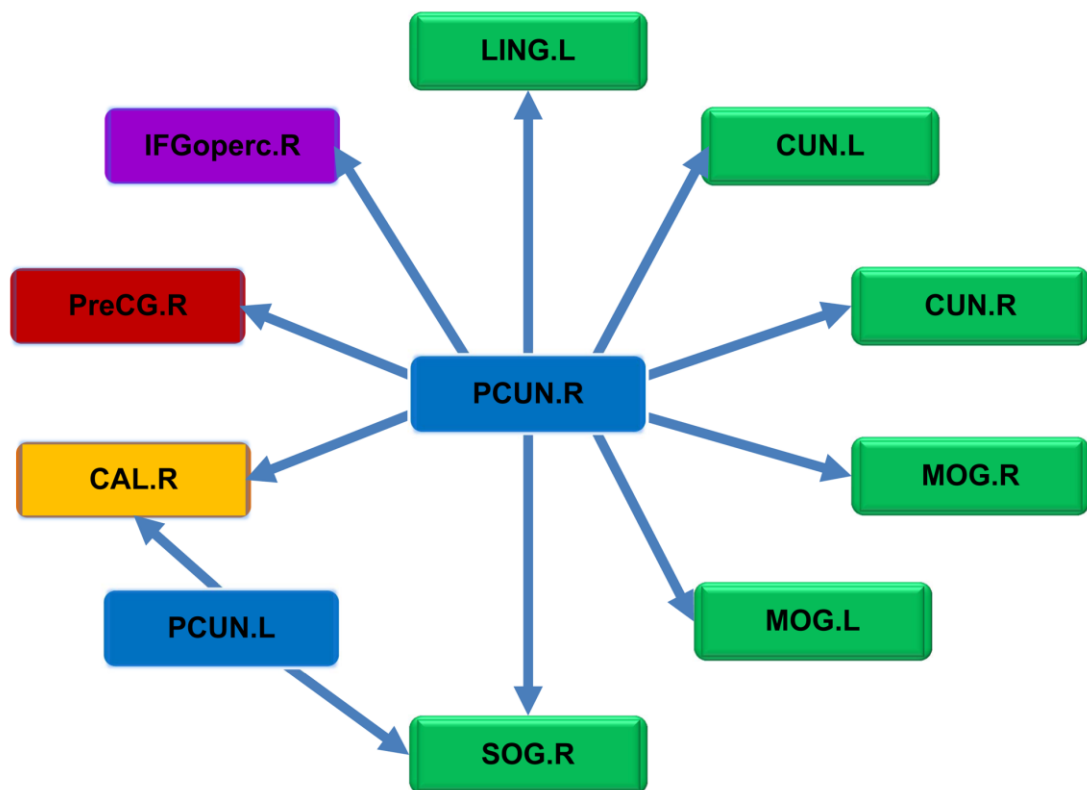


Figure 8. Information flows from precuneus inferred by the average Granger causality based on the optimal time window dividing algorithm. Brain regions for visual recognition are marked in green, primary visual cortex marked in yellow, sensory motor areas marked in red, attention areas in purple. The brain regions are defined by

AAL90 as in DPARSF(Yan and Zang, 2010).

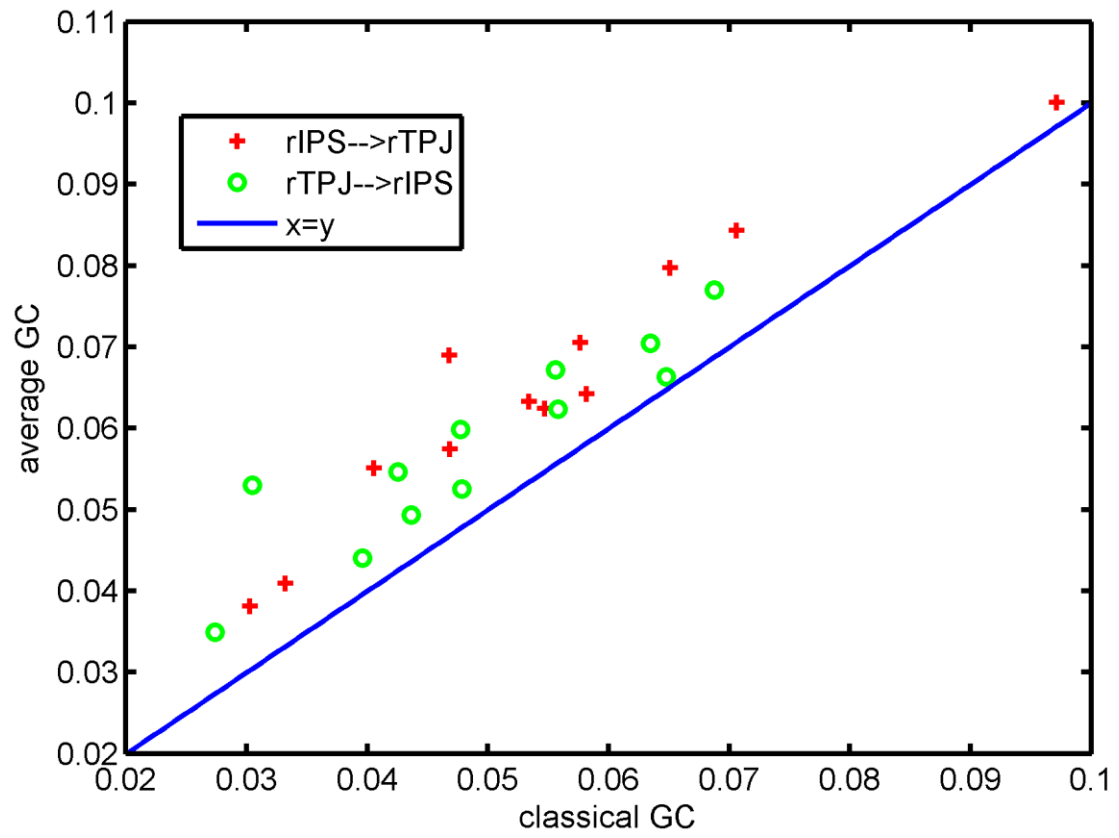


Figure 9. Comparison between the classic Granger causality (classical GC) and the average Granger causality (average GC) for the attention-task dataset.